Differences in mitochondrial activity trigger cell competition during early mouse development

Ana Lima[1,2,#] Gabriele Lubatti[3,4,5,#], Jörg Burgstaller[6], Di Hu[7], Alistair Green[8], Aida Di Gregorio[1], Tamzin Zawadzki[1], Barbara Pernaute[1,9], Elmir Mahammadov[3,4,5], Marian Dore[2], Juan Miguel Sanchez[1], Sarah Bowling[1], Margarida Sancho[1], Mohammad Karimi[2], David Carling[2], Nick Jones[8], Shankar Srinivas[7], Antonio Scialdone[3,4,5*] and Tristan A. Rodriguez[1,*]

[1] National Heart and Lung Institute, Imperial College London, UK

[2] MRC London Institute of Medical Sciences (LMS), Institute of Clinical Sciences, Imperial College London, UK

[3] Institute of Epigenetics and Stem Cells, Helmholtz Zentrum München, Munich, Germany

[4] Institute of Functional Epigenetics, Helmholtz Zentrum München, Neuherberg, Germany

[5] Institute of Computational Biology, Helmholtz Zentrum München, Neuherberg, Germany

[6] Institute of Animal Breeding and Genetics, University of Veterinary Medicine, Vienna, Austria

[7] Department of Physiology, Anatomy and Genetics, University of Oxford, Oxford, UK

[8] Department of Mathematics, Imperial College London, UK.

[9] Current address: Centre for Genomic Regulation (CRG), The Barcelona Institute of Science and Technology, Dr. Aiguader 88, Barcelona 08003, Spain

[#] Both these authors contributed equally

* Authors for correspondence: antonio.scialdone@helmholtz-muenchen.de; tristan.rodriguez@imperial.ac.uk

Summary

Cell competition is emerging as a quality control mechanism that eliminates unfit cells in a wide range of settings from development to the adult. However, the nature of the cells normally eliminated by cell competition and what triggers their elimination remains poorly understood. Here we have performed single cell transcriptional profiling of early mouse embryos and find that the cells eliminated show the hallmarks of cell competition, are mis-patterned and have mitochondrial defects. We demonstrate that mitochondrial defects are common to a range of different loser cell types and that manipulating mitochondrial function is sufficient to trigger competition. Importantly, we show that in the embryo loser epiblast cells display mitochondrial DNA mutations and that even small changes in mitochondrial DNA sequence can influence the competitive ability of the cell. Our results therefore suggest that cell competition is a purifying selection that optimises metabolic output prior to gastrulation.

Running title: Cell competition and mitochondrial selection

Keywords: mitochondria, mtDNA, mouse development, cell competition, purifying selection

Introduction

During the early stages of mammalian development, the cellular and molecular landscape is profoundly remodelled. As embryonic cells approach gastrulation, when the precursors of all embryonic tissues are specified, they need to rewire the transcriptional, epigenetic, metabolic and signalling networks that govern cell identity (Kojima et al., 2014). These changes are accompanied by a marked acceleration in the proliferation rate (Snow, 1977) and need to be orchestrated with the different morphogenetic processes that re-shape the embryo (reviewed in (Stower and Srinivas, 2018). The scale of this remodelling creates the potential for the emergence of abnormal cells that need to be removed to prevent them from contributing to the soma or germline during development. This requirement implies that there must be stringent cell fitness quality control mechanisms acting around the time of gastrulation. One such control has been postulated to be cell competition, a fitness sensing mechanism eliminating cells that, although viable, are less fit than their neighbours (reviewed in (Bowling et al., 2019; Diaz-Diaz and Torres, 2019; Madan et al., 2018). During cell competition, the cells that are eliminated are generically termed losers, while the fitter cells that survive are referred to as winners.

Cell competition has been primarily studied in *Drosophila*, where it was first described in the imaginal wing disc (Morata and Ripoll, 1975). Since then, it has also been found to be conserved in mammals. For example, in the mouse embryo between E5.5 and E6.5 cell competition has been proposed to eliminate less-fit cells from the epiblast, the pluripotent tissue that generates the three primary germ-layers (Claveria et al., 2013; Sancho et al., 2013). Importantly, in the time-window when cell competition acts, about one third of epiblast cells are eliminated by apoptosis (Bowling et al., 2018). These cells are marked by a loss of mTOR signalling, a read-out of loser status during cell competition *in vitro* (Bowling et al., 2018). This suggests that cell competition is the primary cause of this cell elimination. Other markers of those cells eliminated in the early post-implantation embryo have been identified as relative low c-MYC expression, high P53 expression or elevated levels of ERK phosphorylation (Bowling et al., 2018; Claveria et al., 2013; Diaz-Diaz et al., 2017; Sancho et al., 2013), that together could be considered as a cell competition signature.

In spite of the advance that identifying these markers signifies, we still do not know what overarching cellular and molecular features define the cells eliminated by cell competition in mouse. Using embryonic stem cells (ESCs) and embryo chimeras we have shown that mis-patterned cells, autophagy deficient cells and karyotypically abnormal cells are all eliminated upon differentiation by cell competition (Bowling et al., 2018; Sancho et al., 2013). Cell competition has also been shown to eliminate pluripotent cells that differentiate precociously (Diaz-Diaz et al., 2017) or that are not properly specified (Hashimoto and Sasaki, 2019). Therefore, a variety of different defective cell types can be eliminated by cell competition, but which is the underlying cause for their elimination remains poorly understood.

Mitochondria, with their diverse cellular functions ranging from determining the bioenergetic output of the cell to regulating its apoptotic response, are strong candidates for determining competitive cell fitness. During early mouse development mitochondria undergo profound changes in their shape and activity (reviewed in (Lima et al., 2018). In the pre-implantation embryo mitochondria are rounded, fragmented and contain sparse cristae, but upon implantation they fuse to form complex networks with mature cristae (Zhou et al., 2012). The mode of replication of the mitochondrial genome (mtDNA), that encodes for vital components of the bioenergetic machinery, also changes during early mouse development. After fertilization, mtDNA replication ceases and its copy number per cell decreases with every division until post-implantation stages, when mtDNA replication resumes (reviewed in (Lima et al., 2018). However, as the mutation rate of mtDNA is significantly higher than that of nuclear DNA (Allio et al., 2017; Khrapko et al., 1997) this increased replication most likely leads to an increased mutation load. A number of mechanisms have been proposed to reduce this mutation load, such as the bottleneck effect, purifying selection or biased segregation of mtDNA haplotypes (Burgstaller et al., 2014; Johnston et al., 2015; Latorre-Pellicer et al., 2019; Lee et al., 2012; Sharpley et al., 2012; Zhang et al., 2018). However, despite these mechanisms, inheritable mtDNA based diseases are reported with a prevalence of 5-15 cases per 100,000 individuals (Burgstaller et al., 2015; Gorman et al., 2016), highlighting both the importance and limitations of these selection mechanisms.

To understand the nature of the cells eliminated during early mouse post-implantation development we have analysed their transcriptional profile by single-cell RNA sequencing. Importantly, we have found that these cells share a cell competition signature. Analysis of the pathways mis-regulated in the cells eliminated identified mitochondrial dysfunction as a common feature. Furthermore, we demonstrate that manipulating mitochondrial activity either by disrupting mitochondrial dynamics or by introducing small mtDNA changes is sufficient to trigger cell competition during early mouse development. These results therefore pinpoint mitochondrial performance as a key cellular feature that determines the competitive ability of embryonic cells.

Results

Cells eliminated in the early mouse embryo have a distinct transcriptional profile

We have previously shown that in the early post-implantation mouse embryo about 35% of epiblast cells are eliminated and that these cells are marked by low mTOR signalling (Bowling et al., 2018). However, we currently do not understand the characteristics of these cells or what triggers their elimination. To answer these questions, we have analysed their transcriptional profile by single cell RNA sequencing (scRNA-seq). To ensure we can capture the eliminated cells, as we have done before (Bowling et al., 2018), we isolated embryos at E5.5 and cultured them for 16 hours in the presence of a caspase inhibitors (CI) or vehicle (DMSO) (Figure 1A and Figure S1A).

Unsupervised clustering of the scRNA-seq data revealed five clusters: two corresponding to extra-embryonic tissues (visceral endoderm and extra-embryonic ectoderm) and three that expressed epiblast marker genes (Figure 1B-C and Figure S1B-D). Interestingly, cells from CI- and DMSO-treated embryos are unequally distributed across the three epiblast clusters. In particular, one of these clusters (cluster 4) is only composed of cells from CI-treated embryos (Figure 1D-E). To establish the relationship between these epiblast clusters we computed a diffusion map (Angerer et al., 2016). For this, we selected only cells captured from CI-treated embryos, to eliminate possible confounding effects due to the caspase inhibitor (Figure 2A). However, when all epiblast cells are considered, the results remain unchanged (Figure S2A-C). This analysis identified a trajectory between the three epiblast clusters, with those cells unique to CI-treated embryos falling at one extreme end of the trajectory (corresponding to cluster 4; Figure 2A) and with those cells present in both DMSO and CI-treated embryos at the other (corresponding to cluster 1; Figure 2A and Figure S2A-C).

To further define the identity of the epiblast cells of CI-treated embryos we analysed the genes differentially expressed along the trajectory (see Methods and Figure S2D) using Ingenuity Pathway Analysis (IPA) to characterize gene signatures (Kramer et al., 2014). Importantly, we found that these differentially expressed genes fell under molecular and cellular function categories associated with cell death and survival, protein synthesis and nucleic acids (Figure 2B). Analysis of the factors with enriched targets within the genes differentially expressed along the trajectory revealed RICTOR (an mTOR component), TLE3, MYC, MYCN, P53 and IGFR (that is upstream of mTOR) as the top upstream regulators (Figure 2C). Breaking down the differentially expressed genes into those down-regulated or up-regulated along the winner-to loser trajectory revealed that the targets of RICTOR, MYC, MYCN and IGFR primarily fell within the down-regulated genes (Supplementary Tables 1 and 2). P53 activated targets were preferentially up-regulated and P53 repressed targets were preferentially down-regulated (Figure S2E-F). Moreover, genes related to protein synthesis were primarily found to be downregulated.

The first identified trigger of cell competition were differences in protein synthesis (Morata and Ripoll, 1975), therefore the observation that the genes differentially expressed along the trajectory fall into cell death and protein synthesis categories, as well as being mTOR, MYC and P53 targets strongly suggests that cells at each end of the trajectory are the winners and losers of cell competition. For this reason, we hereafter refer to those epiblast cells unique to CI-treated embryos as “loser” epiblast cells and to those at the opposite end of the trajectory as the “winner” epiblast cells. Those cells lying between these two populations on the trajectory are considered “intermediate”. Using this knowledge we can define a diffusion pseudotime (dpt) coordinate (Haghverdi et al., 2016) originating in the “winner” cluster that tracks the position of cells along the

trajectory and that can be interpreted as a "losing score", i.e., it quantifies how strong the signature of the "losing" state is in the transcriptome of a cell (see Figure 2D-E).

Loser cells show a signature of mis-patterning

The most notable change that embryonic cells undergo during early development is the onset of differentiation. During this process cells transit from naïve to primed pluripotency and then undergo germ layer specification (Nichols and Smith, 2009). For this reason, we analysed the expression of pluripotency and differentiation markers as a function of the losing score of epiblast cells (Figure 2F). We found that loser cells (with high losing scores) have lower levels of expression of genes such as *Fgf5* and *Tdgf1*, which are characteristic of the primed pluripotency state. In contrast to this, they displayed high levels of expression of some naïve pluripotency markers such as *Klf4* and *Klf5*, but not of others, such as *Rex1* (*Zfp42*). Analysis of lineage specific markers revealed a complex pattern. For example, some loser cells showed high expression of the endoderm marker *Sox17*, but not of *Gata6*. Something similar was observed for neuroectoderm markers, whereby loser cells showed significantly higher expression of *Neurod1* than winner cells, but comparable levels of *Sox1*.

Plotting the levels of markers of naïve pluripotency and germ layers against each other for single cells revealed that some loser epiblast cells expressed higher levels of both naïve pluripotency and germ-layer markers than normal epiblast cells (Figure 2G). Together, these data suggest that loser epiblast cells represent a generic mis-patterned state, rather than precocious or delayed differentiation.

Loser cells are characterised by defects in mitochondrial function

We next analysed using IPA the cellular pathways mis-regulated in loser epiblast cells and found that the top two pathways (mitochondrial dysfunction and oxidative phosphorylation) are related to mitochondrial function (Figure 3A). Detailed inspection of the oxidative phosphorylation signature in loser versus normal epiblast cells indicated that 92.6% of the genes in this pathway were mis-regulated (Figure 3A), including the majority of genes encoding proteins of the five complexes (Complexes I to V) of the electron transport chain (ETC)(Figure 3B), that were down-regulated along the winner-to-loser trajectory (Supplementary Table 1). For example, we found a down-regulation along the winner to loser trajectory of the mitochondrial DNA encoded *mt-Nd3* and *mt-Atp6* (Figure 3C), of regulators of mitochondrial dynamics such as *Opa1,* as well as of genes involved in mitochondrial membrane and cristae organisation such as *Samm50*, (Figure 3C).

A recent body of evidence has revealed that stress responses, such as the integrated stress response (ISR) or the closely related unfolded protein response (UPR), when triggered in cells with impaired mitochondrial function prompt a transcriptional program to restore cellular

homeostasis (Melber and Haynes, 2018; Munch, 2018; Topf et al., 2016). We observed that loser epiblast cells displayed a characteristic UPR-ISR signature (Figure S3A-C) (Mouchiroud et al., 2013; Nargund et al., 2012; Quiros et al., 2016; Zhao et al., 2002) and key regulators of this response, such as *Atf4, Ddit3*, *Nrf2* and *Foxo3* were all up-regulated in these cells (Figure S3D). Similarly, *Sesn2*, a target of p53 that controls mTOR activity (Saveljeva et al., 2016), was also up-regulated in loser cells (Figure S3D). These findings support the possibility that loser epiblast cells present mitochondrial defects, leading to the activation of a stress response in an attempt to restore cellular homeostasis (Yun and Finkel, 2014).

To validate the significance of the mitochondrial defects observed, we did two things. First, we asked if the changes observed at the mRNA level are also reflected at the protein level. We observed that in CI-treated embryos, loser cells that persist and are marked by low mTOR activity (Bowling et al., 2018), also show significantly lower OPA1 levels (Figure 3D-F). This finding is in agreement with the observation that OPA1 levels are decreased during mitochondrial stress (Quiros et al., 2017). We also found that DMSO-treated embryos showed strong DDIT3 staining (an UPR-ISR marker) in the dying cells that accumulate in the proamniotic cavity, and that in CI-treated embryos, DDIT3 expression was up-regulated in a proportion of epiblast cells (Figure S3E-G). The second thing we did to validate the importance of the mitochondrial defects observed was to study in loser epiblast cells the mitochondrial membrane potential ($\Delta\psi m$), an indication of mitochondrial health. We observed that while the cells of DMSO-treated embryos showed a high $\Delta\psi m$ that fell within a narrow range, in CI-treated embryos the proportion of cells with a low $\Delta\psi m$ significantly increased (Figure 3D and 3G-H). Together, these results suggest that loser epiblast cells have impaired mitochondrial activity that triggers a stress response.

Mitochondrial dysfunction is common to different types of loser cells

The above data indicate that loser epiblast cells are mis-patterned and show mitochondrial defects. To address if mitochondrial defects are a common feature of mis-patterned cells we analysed ESCs that are defective for BMP signalling (*Bmpr1a*$^{-/-}$), as these are abnormally patterned (Di-Gregorio et al., 2007) and eliminated by cell competition (Sancho et al., 2013). In parallel, to determine if mitochondrial defects are present in other loser cells eliminated by cell competition, we also studied tetraploid cells (4n) (Sancho et al., 2013). We first carried out a mass spectrometry analysis using the Metabolon platform and found that metabolites and intermediates of the TCA cycle, such as malate, fumarate, glutamate and α-ketoglutarate are depleted in both *Bmpr1a*$^{-/-}$ and 4n ESCs in differentiation culture conditions (Figure 4A). Next, we performed an extracellular flux Seahorse analysis of *Bmpr1a*$^{-/-}$ ESCs to measure their glycolytic and oxidative phosphorylation (OXPHOS) rates. We observed that when these cells are maintained in pluripotency culture conditions, that are not permissive for cell competition (Sancho *et al.*, 2013), they showed a similar glycolytic activity, but a higher OXPHOS rate than control cells (Figure S4A-

D). In contrast, when *Bmpr1a*$^{-/-}$ cells are induced to differentiate, this phenotype is reversed, with mutant cells showing lower ATP generated through OXPHOS and a higher glycolytic capacity than controls (Figure 4B-E; Figure S4E-F). This suggests that upon differentiation *Bmpr1a*$^{-/-}$ cells are unable to sustain proper OXPHOS activity.

To further test the possibility that defective ESCs have impaired mitochondrial function, we assessed their $\Delta\psi m$. We found that whilst *Bmpr1a*$^{-/-}$ and 4n cells had a similar $\Delta\psi m$ to control cells in pluripotency conditions (Figure S4G-H), upon differentiation both these cell types presented a loss of $\Delta\psi m$, irrespective of whether they were separate or co-cultured with wild-type cells (Figure 4F-G). This reduction in $\Delta\psi m$ is unlikely to be due to excessive mitochondrial reactive oxygen species (ROS) production or to a lower mitochondrial mass within mutant cells since, as for example, *Bmpr1a*$^{-/-}$ cells have lower ROS levels and similar TOMM20 and mt-CO1 expression as control cells (Figure 4H-J; Figure S4I). The fact that the loss of $\Delta\psi m$ and lower OXPHOS activity can be observed even when loser cells are cultured separately, suggests that the mitochondrial dysfunction phenotype is an inherent property of loser cells and not a response to them being out-competed. These results also indicate that the mitochondrial defects are directly linked to the emergence of the loser status: in conditions that are not permissive for cell competition (pluripotency) mutant cells do not show defective mitochondrial function, but when they are switched to differentiation conditions that allow for cell competition, they display impaired mitochondrial function.

To further explore the relationship between mitochondrial activity and the competitive ability of the cell, we analysed the $\Delta\psi m$ of BMP defective cells that are null for p53 (*Bmpr1a*$^{-/-}$*; p53*$^{-/-}$ ESCs), as these are not eliminated by wild-type cells (Bowling et al., 2018). Remarkably, we observed that mutating *p53* in *Bmpr1a*$^{-/-}$ cells not only rescues the loss of $\Delta\psi m$ of these cells, but also causes hyperpolarisation of their mitochondria (Figure 4K). These results strongly support a pivotal role for mitochondrial activity in cell competition.

Impaired mitochondrial function is sufficient to trigger cell competition

The mitochondrial defects observed in loser cells led us to ask if disrupting mitochondrial activity alone is sufficient to trigger cell competition. During the onset of differentiation, mitochondria go from having a fragmented shape to fusing and forming complex networks (reviewed in (Lima et al., 2018). We therefore tested if disrupting mitochondrial dynamics induces cell competition. MFN1 and MFN2 regulate mitochondrial fusion and DRP1 controls their fission (Chen et al., 2003; Prudent and McBride, 2017; Smirnova et al., 2001). We generated *Drp1*$^{-/-}$ ESCs, that show hyper-elongated mitochondria, and *Mfn2*$^{-/-}$ ESCs, that have enlarged globular mitochondria (Figure 5A). Analysis of the *Drp1* mutant cells showed that although they did not grow significantly slower than wild-type cells when cultured separately in differentiation inducing conditions, they were out-

competed by wild-type cells in co-culture (Figure 5B). In contrast to this, we observed that *Mfn2*$^{-/-}$ ESCs displayed very poor growth upon differentiation (data not shown). For this reason, we tested their competitive ability in pluripotency conditions, that we have previously found not to induce the out-competition of *Bmpr1a*$^{-/-}$ or 4n cells (Sancho et al., 2013). Interestingly, we found that although *Mfn2*$^{-/-}$ cells grow similarly to wild-type cells in separate cultures, they were out-competed in co-culture (Figure 5C). The observation that disrupting mitochondrial dynamics can induce cell competition even in pluripotency culture conditions, suggests that mitochondrial activity is a dominant parameter determining the competitive ability of the cell.

Loser epiblast cells accumulate mtDNA mutations

There is strong evidence for selection against aberrant mitochondrial function induced by deleterious mtDNA mutations in mammals (Fan et al., 2008; Freyer et al., 2012; Kauppila et al., 2016; Sharpley et al., 2012; Stewart et al., 2008). Given that we observe that cell competition selects against cells with impaired mitochondrial function, we asked if cell competition could be reducing mtDNA heteroplasmy (frequency of different mtDNA variants) during mouse development. It has been recently shown that scRNA-seq can be used to reliably identify mtDNA variants, although with a lower statistical power compared to more direct approaches, like mtDNA sequencing (Ludwig et al., 2019). We therefore tested if mtDNA heteroplasmy is present in our scRNA-seq data and whether this is associated with the losing score of a cell. Our analysis revealed that the frequency of specific mtDNA polymorphisms increased with the losing score of epiblast cells (Figure 6A), and such mtDNA changes occurred within *mt-Rnr1* and *mt-Rnr2* (Figure 6B-H and Figure S5A-E). Moreover, these changes were not dependant on the litter from which the embryo came from (Figure S5F-K). The mutations we detected in *mt-Rnr1* and *mt-Rnr2* strongly co-occurred in the same cell, with those closest together having the highest probability of co-existing (Figure 6I and Figure S5L). This is suggestive of mtDNA replication errors that could be 'scarring' the mtDNA, disrupting the function of *mt-Rnr1* (12S rRNA) and *mt-Rnr2* (16S rRNA) and causing the loser phenotype. Importantly, the presence of these specific mtDNA mutations in the loser cells suggests that cell competition is contributing to the elimination of deleterious mtDNA mutations during early mouse development.

Changes in mtDNA sequence can determine the competitive ability of a cell

To explore this possibility further we analysed if alterations in mtDNA can induce cell competition by testing the competitive ability of ESCs with non-pathological differences in mtDNA sequence. For this we compared the relative competitive ability of ESCs that shared the same nuclear genome background but differed in their mitochondrial genomes by a small number of non-pathological sequence changes. We derived ESCs from hybrid mouse strains that we had previously engineered to have a common nuclear C57BL/6N background, but mtDNAs from

different wild-caught mice (Burgstaller et al., 2014). Each wild-derived mtDNA variant (or haplotype) contains a specific number of single nucleotide polymorphisms (SNPs) that lead to a small number of amino acid changes when compared to the C57BL/6N mtDNA haplotype. Furthermore, these haplotypes (BG, HB and ST) can be ranked according to their genetic distance from the C57BL/6N mtDNA (Figures 7A and S6A). Characterization of the isolated ESCs revealed that they have a range of heteroplasmy (mix of wild-derived and C57BL/6N mtDNAs) that is stable over several passages (Figure S6B). Importantly, these different mtDNA haplotypes and different levels of heteroplasmy do not alter cell size, cell granularity, mitochondrial mass or mitochondrial dynamics, nor do they substantially impact the cell's $\Delta\psi m$ (Figure S6C-F).

When we tested the competitive ability of these mtDNA ESCs we observed that cells carrying the mtDNAs that are most distant from the C57BL/6N mtDNA, such as the HB(100%), the HB(24%) and the ST(46%) ESCs could all out-compete the C57BL/6N line (Figure 7B-C and S6G). Similarly, when we tested the HB(24%) line against the BG(99%) or the BG(95%) lines (that have mtDNAs more closely related to the C57BL/6N mtDNA), we found that cells with the HB haplotype could also out-compete these ESCs (Figure 7D and S6H). In contrast, we observed that the HB(24%) ESCs were unable to out-compete either their homoplasmic counterparts, HB(100%), or the ST(46%) cells that carry the most distant mtDNA from C57BL/6N (Figure 7E and S6I). These results tell us three things. First, that non-pathological differences in mtDNA sequence can trigger cell competition. Second, that a competitive advantage can be conferred by only a small proportion of mtDNA content, as indicated by our finding that HB(24%) behave as winners. Finally, these findings suggest that the phylogenetic proximity between mtDNA variants can potentially determine their competitive cell fitness.

To characterise the mode of competition between different mtDNA cells we focussed on the HB(24%) and the BG(95%) ESCs. Analysis of these cell lines revealed that specifically when co-cultured, the BG(95%) cells display high levels of apoptosis (Figure 7F), indicating that their out-competition is through their elimination. To gain further insight we performed bulk RNA-seq of these cells in separate and co-culture conditions (Figure S6J) and analysed the differentially expressed genes by gene-set enrichment analysis (GSEA). We found that in separate culture the most notable features that distinguish BG(95%) from HB(24%) cells were a down-regulation of genes involved in oxidative phosphorylation and an up-regulation of those associated with cytokine activity (Figure 7G). Interestingly, in the co-culture condition, in addition to these signatures, BG(95%) cells revealed a down-regulation in signature markers of MYC activity and mTOR signalling (Figure 7H), whose downregulation are known read-outs of a loser status during cell competition in the embryo (Bowling et al., 2018; Claveria et al., 2013; Sancho et al., 2013)(Figure 2C). These results suggest that the elimination of loser mtDNA cells occurs through the same mechanism as the out-competition of defective cells in the embryo (Figure 7I).

The finding that the genes down-regulated in BG(95%) cells when co-cultured with HB(24%) cells fell under functional categories relating to mitochondrial function (Figure S7A) led us to analyse the degree of overlap between these genes and the genes differentially expressed along the winner-to-loser trajectory in the embryo. We observed a significant overlap in down-regulated genes (Figure S7B), as well as in the functional components that these genes can be categorised into (Figure S7C). This further highlights the importance of relative mitochondrial activity for determining the competitive ability of embryonic cells.

Discussion

The emerging role of cell competition as a regulator of cell fitness in a wide range of cellular contexts, from the developing embryo to the ageing tissue (reviewed in (Bowling et al., 2019; Diaz-Diaz and Torres, 2019; Madan et al., 2018), has highlighted the importance of understanding what cell types are normally eliminated by this process. With the aim of understanding this question, we have analysed the transcriptional identity of the cells eliminated in the early mouse embryo. We have found not only that they present a cell competition signature, but also that they are mis-patterned and marked by impaired mitochondrial function. Starting from these results, we leveraged *in vitro* models of cell competition to show that: (i) mitochondrial function is impaired in loser cells eliminated by cell competition, and (ii) that differences in mitochondrial activity are sufficient to trigger cell competition in ESCs. Overall, this points to mitochondrial performance as a key determinant of the competitive ability of cells during early mammalian embryonic development. One implication of our findings is that a range of different types of defect, such as mis-patterning, karyotypic abnormalities or mtDNA mutations, all lead to dysfunctional mitochondria at the onset of differentiation and that ultimately it is their impaired mitochondrial function that triggers cell competition, inducing their elimination (Figure 7I).

It is well known that the successful development of the embryo can be influenced by the quality of its mitochondrial pool (reviewed in (Lima et al., 2018). Moreover, divergence from normal mitochondrial function during embryogenesis is either lethal or can lead to the development of mitochondrial disorders (Chinnery and Hudson, 2013). Deleterious mtDNA mutations are a common cause of mitochondrial diseases and during development selection against mutant mtDNA has been described to occur through at least through two mechanisms, the bottleneck effect and intra-cellular purifying selection. The bottleneck effect is associated specifically with the unequal segregation of mtDNAs during primordial germ cell specification, for example as seen in the human embryo (Floros et al., 2018). In contrast to this, purifying selection, as the name implies, allows for selection against deleterious mtDNAs and has been proposed to take place both during development and post-natal life (Burr et al., 2018). Importantly, purifying selection has been found to occur not only at the organelle level, but also at the cellular level (Rajasimha et al., 2008). Our

findings indicate that purifying selection can occur not only at the intra-cellular level but also inter-cellularly (cell non-autonomously). We show that epiblast cells are able to sense their relative mitochondrial activity and that those cells with mtDNA mutations, lower or aberrant mitochondrial function are eliminated. By selecting those cells with the most optimised mitochondrial performance, cell competition would not only prevent cells with mitochondrial defects from contributing to the germline or future embryo, but also ensure optimization of the bioenergetic performance of the epiblast, contributing to the synchronization of growth during early development.

Cell competition has been studied in a variety of organisms, from *Drosophila* to mammals, and it is likely that multiple different mechanisms fall under its broad umbrella (reviewed in (Bowling et al., 2019; Diaz-Diaz and Torres, 2019; Madan et al., 2018). In spite of this, there is considerable interest in understanding if there could be any common feature in at least some of the contexts where cell competition has been described. The first demonstration of cell competition in *Drosophila* was made by inducing clones carrying mutations in the ribosomal gene *Minute* (Morata and Ripoll, 1975) and this has become one of the primary models to study this process. Our finding that that during normal early mouse development cell competition eliminates cells carrying mutations in *mt-Rnr1* and *mt-Rnr2*, demonstrates that in the physiological context mutations in ribosomal genes also trigger cell competition. Furthermore, our observation that mis-patterned and karyotypically abnormal cells show impaired mitochondrial activity indicates that during early mouse development different types of defects impair mitochondrial function and trigger cell competition. Interestingly, mtDNA genes are amongst the top mis-regulated factors identified during cell competition in the mouse skin (Ellis et al., 2019). In the *Drosophila* wing disc oxidative stress, a general consequence of dysfunctional mitochondria, underlies the out-competition of *Minute* and *Mah-jong* mutant cells (Kucinski et al., 2017). Similarly, in Madin-Darby Canine Kidney (MDCK) cells, a loss of $\Delta\psi m$ occurs during the out-competition of RasV12 mutant cells and is key for their extrusion (Kon et al., 2017). These observations raise that possibility that differences in mitochondrial activity may be a key determinant of competitive cell fitness in a wide range of systems. Unravelling what mitochondrial features can lead to cellular differences that can be read between cells during cell competition will be key not only for understanding this process, but also to open up the possibility for future therapeutic avenues in the diagnosis or prevention of mitochondrial diseases.

Acknowledgments

We would like to thank Stephen Rothery for guidance and advice with confocal microscopy. Gratitude also goes to James Elliot and Bhavik Patel for performing cell sorts. Research in Tristan Rodriguez lab was supported by the MRC project grant (MR/N009371/1) and by the British Heart

Foundation centre for research excellence. Ana Lima was funded by a BHF centre of excellence PhD studentship. Shankar Srinivas was funded through Wellcome awards 103788/Z/14/Z and 108438/Z/15/Z.

Author Contributions

A.L. performed most of the experimental wet lab work. J.B. and A.L. derived heteroplasmic mESC lines. J.B. performed heteroplasmy measurements in heteroplasmic mESCs. B.P. generated *Mfn2*$^{-/-}$ and *Drp1*$^{-/-}$ mESCs and J.M.S did characterisation of mitochondria shape and pluripotency status. D.H. performed embryo dissections, treatments and cell dissociation prior to scRNA-seq experiments. G.L. did the bioinformatic analysis of scRNA-seq data. E.M., N.J. and A.G. participated in the analysis of mitochondrial DNA heteroplasmy. A.D.G. performed the metabolomic studies using Metabolon platform and participated in embryo dissections and immunohistochemistry stainings for validation of results obtained by scRNA-seq. M.D, and M.K. performed the bioinformatic analysis of bulk RNA-seq experiments. N.J., S.S. and D.C. participated in the design of experimental work and analysis of results. A.L., G.L., A.S and T.R. interpreted results and wrote the paper. T.R. and A.S. directed and designed the research.

Declaration of Interests

The authors declare no competing interests.

Figure titles and legends

Figure 1. Cells eliminated during early mouse embryogenesis have a distinct transcriptional profile.

(A) Experimental design. The number of cells in the two conditions (DMSO-treated and CI-treated) refers to the number of cells that passed the quality control.

(B) Identification of the clusters according to known gene markers from the different embryonic regions. Three clusters (clusters 1, 3 and 4) show marker genes of the epiblast (Epi), while the remaining clusters correspond to the extra-embryonic lineages visceral endoderm (VE; cluster 5) and extraembryonic ectoderm (ExE; cluster 2). The epiblast clusters are named “Winner”, “Intermediate” and “Loser” on the basis of the relative fraction of cells from CI-treated embryos they include (see panel E).

(C-D) UMAP visualization of the single-cell RNA-seq data, with cells coloured according to cluster (C) or condition (D). A region made up exclusively by cells from CI-treated embryos emerges.

(E) Ratio between the fraction of cells from DMSO-treated and CI-treated embryos in the three epiblast clusters. While the “winner” epiblast cluster shows an enrichment of cells from DMSO-treated embryos, the “intermediate” and the “loser” epiblast clusters are strongly enriched for cells from CI-treated embryos.

See also Figure S1

Figure 2. A cell competition transcriptional signature is identified in cells eliminated during mouse embryonic development

(A) Diffusion map of epiblast cells (only from CI-treated embryos), coloured by cluster.

(B-C) IPA run on the list of genes differentially expressed along the diffusion trajectory (see Figure S2D) generated lists of top 5 molecular and cellular functions (B) and upstream regulators (C) found to be differentially activated in epiblast cells along the diffusion trajectory from winner (cluster 1) to loser status (cluster 4).

(D) Diffusion map of epiblast cells (only from CI-treated embryos) colored by diffusion pseudotime coordinate (dpt). The winner and the loser clusters are found at the two extremities of the trajectory, hence the dpt can be interpreted as a “losing score”.

(E) Losing score of the cells in the three epiblast clusters in CI-treated (left) or DMSO-treated (right) embryos. The losing score of the cells from DMSO-treated embryos was obtained by projecting them on the diffusion map shown in panel D (see Methods).

(F) Expression levels of genes (in rows) that are markers for naïve pluripotency (*Klf4* and *Klf5*), primed pluripotency (*Fgf5* and *Tdgf1*), mesoderm (*Mesp1* and *T*), neuroectoderm (*Neurod1* and *Sox1*) and endoderm (*Sox17*). Cells (in columns) are sorted by their losing scores. The genes marked with a * are differentially expressed along the trajectory.

(G) Scatter plots of the expression levels of different marker genes in cells from the loser epiblast cells (cluster 4), suggesting that loser cells are mis-patterned.
See also Figure S2.

Figure 3. Cells eliminated during early mouse embryogenesis have mitochondrial defects.
(A) Top canonical pathways, identified by IPA, mis-regulated in loser cells in comparison to normal epiblast cells. The numbers at the end of each bar refer to total amount of genes involved in that pathway. The percentage refers to the number of genes found mis-regulated relative to the number total genes within each pathway. Statistical significance calculated with Fisher's exact test ($p<0.05$): Mitochondrial Dysfunction, -log10(p-value) = 21.1; Oxidative Phosphorylation, - log10(p-value) = 18.6; EIF2 signalling, - log10(p-value) = 11.9.
(B) Detail of changes in oxidative phosphorylation pathway identified in (A). Circular and oval shapes represent each of the ETC complexes (complexes I to V). Diamond shapes represent subunits of each ETC complex. Genes that are differentially expressed between loser and winner epiblast cells are colored in shades of red, with darker shades corresponding to lower values of FDR, which ranges from 1.25E-51 (for *Atp5b*) to 5.42E-03 (for *Ndufa11*). Grey color denotes genes that were not significant (FDR>0.01). White color denotes genes from the Knowledge Base that were not tested (e.g., because they were not detected in our dataset).
(C) Expression levels of some mitochondrial genes as a function of cells' losing score. *mt-Atp6*, mitochondrial DNA encoded ATP synthase membrane subunit 6; *mt-Nd3*, mitochondrial DNA encoded NADH dehydrogenase subunit 3; *Opa1*, optic atrophy 1; *Samm50*, sorting and assembly machinery component 50 homolog.
(D) Experimental design adopted to assess mitochondria function (OPA1 expression, by immunofluorescence or Δψm, given by TMRM fluorescence) in epiblast cells from embryos where cell death was allowed (DMSO-treated) or inhibited (CI-treated). * Micrograph of isolated epiblast (arrow) after embryo microdissection.
(E) Representative immunohistochemistry of OPA1 in E6.5 embryo where cell death was inhibited (CI-treated), quantified in (F). Loser cells are identified by low mTOR activation (low p-rpS6, arrowheads). Scale bar = 20 μm.
(F) Quantification of OPA1 fluorescence in normal epiblast cells and loser cells. N=6 embryos with a minimum of 8 cells analysed per condition. Statistical analysis performed by Mann-Whitney test.
(G) Representative histogram of flow cytometry analysis of TMRM probe, indicative of Δψm, in epiblast cells from embryos where cell death was allowed (DMSO-treated) or inhibited (CI-treated), quantified in (H).
(H) Frequency of epiblast cells with high or low TMRM fluorescence, according to range defined in (G) from embryos where cell competition was allowed (DMSO treated) or inhibited (CI-treated). Statistical analysis done by two-way ANOVA, followed by Holm-Sidak's multiple comparisons test.

N=3 independent experiments. Data shown as mean ± SEM.
See also Figure S3.

Figure 4. Mitochondrial defects are a common feature of cells eliminated by cell competition.

(A) Metabolic enrichment analysis of the TCA cycle and intermediate metabolites obtained using Metabolon platform for defective cells (*Bmpr1a*$^{-/-}$, left bar and 4n, right bar), in comparison to wild-type cells during differentiation. Bars indicate compound levels relative to wild-type cells. Blue bars indicate compounds that are significantly depleted ($p<0.05$) and light blue bars indicate compounds that are almost significantly depleted ($0.05\leq p\leq 0.1$). Black bars indicate compounds that are depleted although not statistically significant in comparison to the levels found in wild-type cells. The enzymes on the pathway are represented as boxes and labelled by their canonical names.
(B-E) Metabolic flux analysis of wild-type and BMP-defective cells during differentiating conditions. Statistical analysis done with Mann-Whitney test. Analysis of oxygen consumption rate (OCR) as a measure of mitochondria function (mitochondria stress test) (B). Detail of metabolic parameters found changed from the analysis of the mitochondria stress test (C). Analysis of extracellular acidification rate (ECAR) as a measure of glycolytic function (glycolysis stress test) (D). Detail of metabolic parameters found changed from the analysis of the glycolysis stress test (E).
(F-G) Analysis of mitochondrial membrane potential (Δψm) in defective mESCs undergoing differentiation in separate or co-culture conditions. Representative histograms of TMRM fluorescence and quantification for wild-type and *Bmpr1a*$^{-/-}$ (F) and wild-type and 4n (G). Statistical analysis done by two-way ANOVA, followed by Holm-Sidak's multiple comparisons test.
(H) Representative micrographs of wild-type and *Bmpr1a*$^{-/-}$ cells co-cultured during differentiation and stained for marker of Δψm (MitoTracker Red, top panel) or mitochondria mass (TOMM20, bottom panel). Nuclei are stained with Hoechst. Scale bar = 10 μm.
(I-J) Western blot analysis of mitochondria mass markers TOMM20 (I) and mt-CO1 (J) for wild-type and *Bmpr1a*$^{-/-}$ cells during differentiation. Statistical analysis done with Mann-Whitney test.
(K) Analysis of mitochondrial membrane potential (Δψm) for wild-type, *Bmpr1a*$^{-/-}$ and *Bmpr1a*$^{-/-}$;*p53*$^{-/-}$ cells during differentiation. Representative histogram of TMRM fluorescence and quantification. Statistical analysis done by one-way ANOVA, followed by Holm-Sidak's multiple comparisons test.
Data shown as mean ± SEM of a minimum of 3 independent experiments.
See also Figure S4.

Figure 5. Manipulating mitochondria biology is sufficient to trigger cell competition.

(A) Representative micrographs of wild-type, *Drp1*$^{-/-}$ and *Mfn2*$^{-/-}$ mESCs showing alterations in mitochondrial morphology in mutant cells. TOMM20 was used as mitochondrial marker and NANOG as a pluripotency marker. Nuclei are stained with Hoechst. Scale bar = 5 μm.
(B-C) Cell competition assays between wildtype mESCs and cells with altered morphology, *Drp1*$^{-/-}$ (B) and *Mfn2*$^{-/-}$ (C). The ratio of final/initial cell numbers in separate or co-culture is shown. Statistical analysis done with two-way ANOVA, followed by Holm-Sidak's multiple comparisons test.

Figure 6. Intermediate and loser epiblast cells accumulate polymorphisms in mtDNA sequence.
(A-G) mtDNA heteroplasmy, *H*, in epiblast cells from CI-treated embryos. Average heteroplasmy (considering all eleven polymorphisms that have a statistically significant dependence on the losing score; see Methods) as a function of cells' losing scores. The p-value was computed with a generalized linear model (A). mtDNA heteroplasmy for six positions within the *mt-Rnr1* gene (B-G). The heteroplasmy at all of these positions as well as the average heteroplasmy increase with the cells' losing scores in a statistically significant way (the adjusted p-value estimated via a generalized linear model is indicated at the top of each plot).
(H) The barplot indicates the fraction of epiblast cells in each of the cluster indicated on the x-axis (winner, intermediate, loser) that carry a mean heteroplasmy *H (*computed on the six positions within the *mt-Rnr1* indicated in the panels B-G) greater than 0.01. This shows that the level of mtDNA heteroplasmy in *mt-Rnr1* is strongly associated with the loser status of the cells, since ~55% and ~87% of cells in the intermediate and the loser clusters, respectively, have heteroplasmic sequences in this gene compared to only ~5% of cells in the winner cluster.
(I) Spearman's correlation coefficient between the mtDNA heteroplasmy at the six positions shown in panels (B-G).
See also Figure S5.

Figure 7. Changes in mtDNA sequence can determine the competitive ability of a cell.
(A) Derivation of mESCs from hybrid mouse strains, generated elsewhere by Burgstaller and colleagues. Neighbour-Joining Phylogenetic Analysis of mtDNA from wild and C57BL/6N mouse strains, that were used to generate hybrid mice (adapted from Burgstaller et al, 2014), illustrates the genetic distance of the mtDNA from wild mouse strains to the C57BL/6N lab mouse. The number of single nucleotide polymorphisms and amino acid changes (SNPs/ a.a. changes) from wild to lab mouse strain is shown. mESCs were derived from embryos of hybrid mice, containing the nuclear background of a C57BL/6N lab mouse and mtDNA from three possible wild-derived strains (BG, HB or ST).

(B-E) Cell competition assays between cells derived from the embryos of hybrid mice. The ratio of final/initial cell numbers in separate or co-culture is shown. Statistical analysis done with two-way ANOVA, followed by Holm-Sidak's multiple comparisons test.
(F) Representative micrographs of cleaved caspase-3 staining and quantification of the percentage of apoptotic events in winners HB(24%) and loser BG(95%) mESCs and cultured in separate or co-culture conditions. Statistical analysis done with two-way ANOVA, followed by Holm-Sidak's multiple comparisons test.
(G-H) Gene set enrichment analysis of differentially expressed genes from bulk RNA seq. in loser loser BG (95%) compared to winner HB (24%) mESCs cultured in separate (J) or co-culture conditions (K). Gene sets that show positive normalized enrichment scores (NES) are enriched in loser cells, while gene sets that show negative NES are depleted in loser cells.
(I) Summary of the main findings of the study. A range of cellular defects, such as aneuploidy, mis-patterning or mtDNA mutations cause alterations in mitochondria function, which affect the relative fitness of cells. The cells with suboptimal mitochondrial activity survive in a homogeneous population, but are eliminated by cell competition in the presence of fitter cells.
Data in panels (B-F) shown as mean ± SEM of a minimum of 3 independent experiments.
See also Figure S6.

Figure S1. Quality controls of scRNA-seq
(A) These boxplots show the log10-total number of reads (top left), the fraction of mapped reads (top central), the fraction of reads mapped to endogenous genes (top right), the fraction of reads mapped to mitochondrial genes (bottom left), the fraction of reads mapped to ERCC spike-ins (bottom central) and the number of genes with more than 10 reads per million (bottom right) for all cells (723) that passed the quality control.
(B) Number of good quality cells in each condition (rows) and batch (columns).
(C) Number of good quality cells per cluster (rows) and batch (columns).
(D) UMAP plot of the data with cells colored by batch. In each batch there is a balanced distribution of cells in the two conditions and across the five clusters.

Figure S2. Analysis on epiblast cells from DMSO and CI-treated embryos
(A-B) Diffusion map analysis in all epiblast cells (from DMSO and CI-treated embryos): cells are coloured according to the condition (A) and to the cluster (B).
(C) The pseudo-time coordinate of the CI-treated epiblast cells obtained from the diffusion map including all epiblast cells correlates extremely well with the pseudo-time coordinate obtained in the diffusion map calculated only from CI-treated epiblast cells (Figure 2A).
(D) Heatmap showing the expression pattern of all genes differentially expressed along the trajectory from winning to losing cells in Figure 2D.

(E-F) Overlap of genes differentially expressed along the trajectory joining winning and losing epiblast cells in CI-treated embryos (Figure 2A and S2D) and genes targeted by p53. Pie charts show the percentage of genes up- or down-regulated in loser cells within the group of target genes that are activated (E) or repressed (F) by p53. There is an enrichment of activated/repressed targets among genes upregulated/downregulated in losing cells respectively (Fisher's test, p-value=1E-4). The list of p53 targets is taken from (Fischer, 2017).

Figure S3. Cells eliminated during early mouse embryogenesis have activated stress responses.

(A) Overlap of genes differentially expressed along the trajectory joining winning and losing epiblast cells in CI-treated embryos (Figure 2A and Figure S2F) and genes related to the unfolded protein response and integrated protein response pathways (UPR_ISR, see Supplementary Table 3). From the 32 genes related to the UPR & ISR pathways, 12 are down-regulated in loser cells, 8 genes are up-regulated in loser cells, and 12 genes are not differentially expressed between loser and winner cells. There is a statistically significant enrichment of UPR&ISR genes among the up-regulated genes in loser cells (Fisher test, odds ratio=3.0, p-value=0.012). The intersection between UPR-ISR genes and the down regulated genes is not significant (Fisher test, odds ratio=1.2, p value=0.69).

(B-C) List of genes from UPR-ISR pathways that are statistically significantly upregulated (B) or downregulated (C) in loser cells.

(D) Scatterplots with the expression levels of genes involved in stress responses in epiblast cells from CI-treated embryos as a function of cells' losing score.

(E) Experimental design with the approach taken to validate the expression of the stress response marker DDIT3 in epiblast cells from DMSO or CI-treated embryos.

(F) Representative micrographs of DMSO (upper panel) or CI-treated embryos (100 μM, lower panel) stained for DDIT3, quantified in (G). Nuclei are labelled with Hoechst. In control embryos (DMSO-treated), dying cells in the cavity show very high DDIT3 expression (arrow), while live cells in the epiblast of the CI-treated embryos show more modest levels of DDIT3 expression (arrowheads). Scale bar = 20 μm.

(G) Quantification of the percentage of epiblast cells with nuclear DDIT3 expression. N=10 DMSO and N=9 CI-treated embryos. Data shown as mean ± SEM.

Ddit3 (Chop), DNA-damage inducible transcript 3; *Atf3*, activating transcription factor 3; *Atf4*, activating transcription factor 4; *Foxo3*, forkhead box O3; *Ppp1r115a (Gadd34),* Protein Phosphatase 1 Regulatory Subunit 15A, *Eif2ak3 (Perk),* Eukaryotic Translation Initiation Factor 2 Alpha Kinase 3; *Nfe2l2 (Nrf2)*, NFE2-related factor 2;. *Sesn2*, Sestrin 2; *Gdf15*, Growth Differentiation Factor 15; *Mthfd1l*, Methylenetetrahydrofolate Dehydrogenase (NADP+ Dependent) 1 Like; *Hspe1*, Heat Shock Protein Family E (*Hsp10*) Member 1; *Cat*, Catalase;

582 *Hspd1*, Heat Shock Protein Family D (Hsp60) Member 1; *Sod2,* Superoxide Dismutase 2; *Hsph1,*
583 Heat Shock Protein Family H (*Hsp110*) Member 1; *Lonp1*, Lon Peptidase 1, Mitochondrial; *Eif2a,*
584 Eukaryotic Translation Initiation Factor 2A; *Mthfd2*, Methylenetetrahydrofolate Dehydrogenase
585 (NADP+ Dependent) 2, Methenyltetrahydrofolate Cyclohydrolase; *Hspa4*, Heat Shock Protein
586 Family A (*Hsp70*) Member 4; *Cth*, Cystathionine Gamma-Lyase; *Nrf1*, Nuclear Factor 1.

587 **Figure S4. Mitochondrial function in Wild-type, *Bmpr1a*$^{-/-}$ and 4n mESCs**
588 (A-F), Metabolic analysis of wild-type and *Bmpr1a*$^{-/-}$ mESCs. OCR profile during the mitochondria
589 stress test performed in pluripotency conditions (A). Metabolic parameters assessed during the
590 mitochondria stress test performed in pluripotency conditions (B). ECAR profile during the
591 glycolysis stress test performed in pluripotency conditions (C). Metabolic parameters assessed
592 during the glycolysis stress test performed in pluripotency conditions (D). Metabolic parameters
593 from the mitochondria stress test found to be similar between wild-type and *Bmpr1a*$^{-/-}$ mESCs
594 during differentiation (E). Metabolic parameters from the glycolysis stress test found to be similar
595 between wild-type and *Bmpr1a*$^{-/-}$ mESCs during differentiation (F).
596 (G-H) Analysis of mitochondrial membrane potential (Δψm) in defective mESCs maintained in
597 pluripotency conditions, in separate or co-culture. Representative histograms of TMRM
598 fluorescence and quantification for wild-type and *Bmpr1a*$^{-/-}$ (G) and wild-type and 4n (H). Statistical
599 analysis done by two-way ANOVA, followed by Holm-Sidak's multiple comparisons test.
600 (I) Analysis of mitochondrial ROS in wild-type and *Bmpr1a*$^{-/-}$ mESCs undergoing differentiation in
601 separate or co-culture: representative histograms of mitoSOX Red fluorescence and quantification
602 of the percentage of mitoSOX positive cells.
603 Data obtained with a minimum of 3 independent experiments. Error bars represent SEM.

604 **Figure S5. Analysis of SNPs in mtDNA in epiblast cells.**
605 (A-E) mtDNA heteroplasmy, *H*, in epiblast cells from CI-treated embryos for five positions within
606 the *mt-Rnr2* gene. All of these positions have an heteroplasmy that increases with the cells' losing
607 scores in a statistically significant way (the adjusted p-value estimated via a generalized linear
608 model is indicated at the top of each plot).
609 (F-K) The variation in the heteroplasmy across the CI-treated cells is not due to a batch effect for
610 the 6 significant positions within the *mt-Rnr1* gene.
611 (L) Spearman's correlation between the mtDNA heteroplasmy at all the statistically significant
612 positions (six within the gene mt-*Rnr1* and five within the gene mt-*Rnr2*).

613 **Figure S6. Changes in mtDNA sequence are enough to trigger cell competition.**
614 (A) Illustration of the process of derivation of the mESCs lines from mice that are hybrid between
615 the wild-caught strains (BG, HB or ST) and the lab mouse (C57BL/6N). These hybrid mice were
616 generated elsewhere (Burgstaller et al, 2014) by ooplasmic transfer: the zygote of a C57BL/6N

mouse was injected with ooplasm from a wild-caught mouse (orange, HB pictured). Therefore, these hybrid mice contain the nuclear background of the C57BL/6N strain and the mtDNA of wild-caught strain and potentially C57BL/6N mtDNA (heteroplasmic mice strains). mESCs lines were derived from the hybrid mice and characterised.

(B-F) Characterisation of cell lines derived by flow cytometry in comparison to the wild-type cell line used in previous experiments (E14, 129/Ola background). Heteroplasmy analysis of the derived mESC lines from the hybrid mice, indicating the percentage of wild-derived mtDNA (B). Cell granularity (internal complexity) given as median fluorescence intensity of SSc-A laser (C). Cell size given as median fluorescence intensity of FSc-A laser (D). Analysis of the expression of mitochondrial markers: representative western blot and quantification of markers of mitochondrial mass (ATPB, mt-CO1 and TOMM20) and mitochondrial dynamics (DRP1, MFN1and MFN2), relative to vinculin, in cells derived from hybrid mice (E). Representative histograms and quantification of median TMRM fluorescence, indicative of Δψm, for the hybrid cell lines derived, in comparison to the wild-type cell line used in previous experiments (E14, 129/Ola background)(F). Statistical analysis done by one-way ANOVA, followed by Holm-Sidak's multiple comparisons test.

(G-I) Cell competition assays between hybrid cell lines. The ratio of final/initial cell numbers in separate or co-culture is shown. Statistical analysis done by two-way ANOVA, followed by Holm-Sidak's multiple comparisons test.

(J) Experimental design for RNA-Seq and GSEA. The isolation of RNA from winner HB(24%) and loser BG(95%) cells was performed after three days in separate or co-culture conditions, once cells have been subjected to FACS to isolate the two populations form mixed cultures.

Data obtained with a minimum of 3 independent experiments. Error bars represent SEM.

Figure S7. Common features of scRNA-seq and bulk RNA-seq datasets.

(A) Terms significantly enriched among genes downregulated in BG(95%) (loser) ESCs *in vitro* when co-cultured with HB(24%) cells. The loss of mitochondrial activity emerges as a common feature between loser cells *in vivo* and *in vitro*. The gene enrichment analysis was performed using g-profiler tool (see Methods).

(B) Intersection between differentially expressed genes along the trajectory from winning to losing epiblast cells (“in_vivo_scRNA-seq”; Figure 2A and S2D) and genes differentially expressed between co-cultured HB(24%) (winner) and BG(95%) (loser) ESCs (“in_vitro_bulk_RNA-seq”). “Up” and “Down” here refer to genes up- or down-regulated in loser cells. Fisher test for the intersection between down-regulated genes from scRNA-seq (*in vivo*) and down-regulated genes from bulk RNA-seq (*in vitro*): p-value, 1.71E-12; odds ratio 1.80. Fisher test for the intersection between down-regulated genes from scRNA-seq (*in vivo*) and up-regulated genes from bulk RNA-seq (*in vitro*): p-value, 5.20E-3; odds ratio 0.67. Fisher test for the intersection between up-

regulated genes from scRNA-seq (*in vivo*) and down-regulated genes from bulk RNA-seq (*in vitro*): Fisher test p-value, 4.87E-3; odds ratio 0.80.The intersection between up-regulated genes from sc-RNA-seq (*in vivo*) and up-regulated genes from bulk RNA-Seq (*in vitro*) is not statistically significant: Fisher test p-value: 0.30, odds ratio 1.14.

(C) Intersection between the significantly enriched terms in genes upregulated or downregulated in loser cells in the epiblast of CI-treated embryos ("*in_vivo*_scRNA-Seq") or in our *in vitro* model of competition between co-cultured HB(24%) (winner) and BG(95%) (loser) ESCs ("*in_vitro*_bulk_RNA-seq"). All the terms enriched among downregulated genes *in vitro* are also enriched *in vivo*.

List of Tables.

Supplementary Table 1. List of genes down-regulated along the winner-to-loser trajectory in the embryo.

Supplementary Table 2. List of genes up-regulated along the winner-to-loser trajectory in the embryo.

Supplementary Table 3. Genes related to the unfolded protein response and integrated protein response pathways (UPR_ISR) that were analysed in the genes differentially expressed along the winner-to-loser trajectory.

Supplementary Table 4. List of background genes for the winner-to-loser trajectory in the embryo.

Supplementary Table 5. List of genes down-regulated in BG(95%) cells when co-cultured with HB(24%) cells.

Supplementary Table 6. List of genes up-regulated in BG(95%) cells when co-cultured with HB(24%) cells.

Supplementary Table 7. List of background genes used for the analysis of genes differentially expressed between co-cultured BG(95%) and HB(24%) cells .

STAR Methods

KEY RESOURCES TABLE

Presented in a separate file

LEAD CONTACT AND MATERIALS AVAILABILITY

Tristan Rodriguez: tristan.rodriguez@imperial.ac.uk and Antonio Scialdone
antonio.scialdone@helmholtz-muenchen.de

EXPERIMENTAL MODEL AND SUBJECT DETAILS

Cell lines and cell culture routine

E14, kindly provided by Prof A. Smith, from Cambridge University, were used as wild-type control cells tdTomato-labelled or unlabelled. GFP-labelled or unlabelled cells defective for BMP signalling (*Bmpr1a*$^{-/-}$), tetraploid cells (4n) and *Bmp1a*$^{-/-}$ null for p53 (*Bmpr1a*$^{-/-}$;*p53*$^{-/-}$) are described elsewhere (Bowling et al., 2018; Sancho et al., 2013). Cells null for Dynamin-related protein 1 (*Drp1*$^{-/-}$) or Mitofusin 2 (*Mfn2*$^{-/-}$) were generated by CRISPR mutagenesis. Cells with different mitochondrial DNA (mtDNA) content in the same nuclear background were derived from embryos of hybrid mice, generated elsewhere (Burgstaller et al., 2014).

Cells were maintained pluripotent and cultured at 37ºC in 5% CO_2 in 25 cm^2 flasks (Nunc) coated with 0.1% gelatin (Sigma) in DPBS. Growth media (ES media) consisted of GMEM supplemented with 10% FCS, 1mM sodium pyruvate, 2 mM L-glutamine, 1X minimum essential media non-essential amino-acids, 0.1 mM β-mercaptoethanol (all from Gibco) and 0.1% leukemia inhibitory factor (LIF, produced and tested in the lab). Cells derived from hybrid mice (C57BL/6N nuclear background) were maintained on 0.2% LIF. The growth media was changed daily, and cells were split every 3 days.

CRISPR mutagenesis

Drp1 and Mfn2 knockout ESCs were generated by CRISPR-Cas9 mediated deletion of Drp1 exon 2 and Mfn2 exon 3 respectively. sgRNA guides flanking Drp1 exon 2 or Mfn2 exon 3 were cloned into the PX459 vector (Addgene)(Ran et al., 2013): Drp1 exon 2 upstream sgRNA: 5' TGGAACGGTCACAGCTGCAC 3'; Drp1 exon 2 downstream sgRNA: 5' TGGTCGCTGAGTTTGAGGCC 3'; Mfn2 upstream sgRNA: 5' GTGGTATGACCAATCCCAGA 3'; Mfn2 downstream sgRNA: 5' GGCCGGCCACTCTGCACCTT 3'. E14 ESCs were co-transfected with 1ug of each sgRNA expression using Lipofectamine 2000 (Invitrogen) according to manufacturer's instructions. As control E14 ESCs were transfected in parallel with equal amount of empty PX459 plasmid. Following 6 days of Puromycin selection, single colonies were picked from both Drp1 sgRNA and empty vector transfected ESCs and screened for mutations. Drp1 exon 2 deletion was confirmed by PCR genotyping using the following primers: Drp1_genot F: 5' GGATACCCCAAGATTTCTGGA 3'; Drp1_genot R: 5' AGTCAGGTAATCGGGAGGAAA 3',

713 followed by Sanger Sequencing. Mfn2 exon 3 deletion was confirmed by PCR genotyping using
714 the following primers: Mfn2_genot F: 5' CAGCCCAGACATTGTTGCTTA 3'; Mfn2_genot R: 5'
715 AGCTGCCTCTCAGGAAATGAG 3', followed by Sanger Sequencing.

716 **Derivation of mESCs from hybrid mouse strains**

717 The derivation of new mESC lines was adapted from (Czechanski et al., 2014). Heteroplasmic
718 mESCs were derived from embryos of hybrid mouse strains BG, HB and ST. These contain the
719 mtDNA of C57BL/6N (Bl6) lab mouse and mtDNA variants from wild-caught mice (Burgstaller et
720 al., 2014).

721 Embryos were isolated at E2.5 (morula stage) and cultured in 4-well plates (Nunc, Thermo
722 Scientific) containing KSOM media (Millipore) plus two inhibitors (KSOM+2i): 1 μM MEK inhibitor
723 PDO325901 (Sigma-Aldrich) and 3 μM GSK-3 inhibitor CHIR9902 (Cayman Chemicals) for 2 days
724 at 37ºC in 5% CO_2 incubator. To reduce evaporation, the area surrounding the wells was filled
725 with DPBS. Embryos were further cultured in a fresh 4-well plates containing, N2B27+2i+LIF
726 media: N2B27 media supplemented with 1 μM MEK inhibitor PDO325901 and 3 μM GSK-3
727 inhibitor and 0.1% LIF for up to 3 days until reaching the blastocyst stage. Each embryo was then
728 transferred to a well of a 96-well plate coated with 0.1% gelatin in DPBS and containing 150 μL of
729 N2B27+2i+LIF media per well. In these conditions, the embryos should attach to the wells allowing
730 the epiblast to form an outgrowth. This plate was then incubated at 37ºC in 5% CO_2 incubator for
731 3 to 7 days until ES-like colonies start to develop from the epiblast outgrowth. Cells were passaged
732 by dissociation with Accutase (Sigma) and seeded in gradual increasing surface area of growth
733 (48-well, 24-well, 12-well plate, T12.5 and T25 flask), until new cell lines were established. At this
734 stage cells were weaned from N2B27+2i+LIF media and then routinely cultured in ES media.

735 **Animals**

736 Mice were maintained and treated in accordance with the Home Office's Animals (Scientific
737 Procedures) Act 1986. All mice were housed on a 10 hr-14 hr light-dark cycle with access to water
738 and food *ad libitum*. Mattings were generally set up in the afternoon. Noon of the day of finding a
739 vaginal plug was designated embryonic day 0.5 (E0.5). Embryo dissection was performed at
740 appropriate timepoints in M2 media (Sigma), using Dumont No.5 forceps (11251-10, FST). No
741 distinction was made between male and female embryos during the analysis.

742 **METHOD DETAILS**

743 **Embryo experiments**

744 Early mouse embryos were isolated at E5.5 (from pregnant CD1 females, purchased from Charles
745 River, UK). Following dissection from the decidua, embryos were cultured overnight in N2B27
746 "poor" media (same formulation as N2B27 media but supplemented with 0.5xB27 supplement and
747 0.5xN2 supplement) with pan-caspase inhibitors (100 μM, Z-VAD-FMK, FMK001, R&D Systems,

USA) or equal volume of vehicle (DMSO) as control. On the next morning, embryos were processed for single cell RNA-Seq (scRNA-seq) or functional validation (Δψm analysis and immunohistochemistry for markers of loser cells).

For the scRNA-seq and Δψm analysis embryos were dissociated into singe-cells. Briefly, up to 12 embryos were dissociated in 600 µL Acccutase (A6964, Sigma, UK) during 12 min at 37ºC, tapping the tube every two minutes. Accutase was then neutralised with equal volume of FCS, cells span down and stained with TMRM, for Δψm analysis, or directly re-suspended in 300 µL DPBS with 1% FCS, for single cell sorting and RNA-seq. Sytox blue (1:1000, S34857, ThermoFisher Scientific, UK), was used as viability staining.

Cell competition assays

Cell competition assays between wild-type and *Bmpr1a*$^{-/-}$, 4n or *Drp1*$^{-/-}$ cells were performed in differentiating conditions. Cells were seeded onto fibronectin-coated plates (1:100, Merck) in DPBS during 1h at 37ºC and grown in N2B27 media - to promote the differentiation of mESCs into a stage resembling the post-implantation epiblast, as cell competition was previously shown to occur in these conditions (Sancho et al., 2013). N2B27 media consisted of 1:1 Dulbecco's modified eagle medium nutrient mixture (DMEM/F12) and Neurobasal supplemented with N2 (1x) and B27 (1x) supplements, 2 mM L-glutamine and 0.1 mM β-mercaptoethanol - all from Gibco. Cell competition assays between wild-type and *Mfn2*$^{-/-}$ and between mESCs with different mtDNA content were performed in pluripotency maintenance conditions (ES media).

Cells were seeded either separately or mixed for co-cultures at a 50:50 ratio, onto 12 well plates, at a density of 8E04 cells per well, except for assays between wild-type and *Mfn2*$^{-/-}$ mESCs, where 3.2E05 cells were seeded per well. The growth of cells was followed daily and compared between separate or co-culture, to control for cell intrinsic growth differences, until the fourth day of culture. Viable cells were counted daily using Vi-CELL XR Analyser (Beckman Coulter, USA), and proportions of each cell type in co-cultures were determined using LSR II Flow Cytometer (BD Bioscience), based on the fluorescent tag of the ubiquitously expressed GFP or TdTomato in one of the cell populations.

Metabolomic Analysis

The metabolic profile was obtained using the Metabolon Platform (Metabolon, Inc). Each sample consisted of 5 biological replicates. For each replicate, 1E07 cells were spun down and snap frozen in liquid nitrogen. Pellets from 5 independent experiments for each condition were analysed by Metabolon Inc by a combination of Ultrahigh Performance Liquid Chromatography-Tandem Mass Spectroscopy (UPLC- MS/MS) and Gas Chromatography-Mass Spectroscopy (GC-MS). Compounds were identified by comparison to library entries of purified standards based on the retention time/index (RI), mass to charge ratio (*m/z)*, and chromatographic data (including MS/MS

spectral data) on all molecules present in the library. Samples were normalized to protein content measured by Bradford assay. Statistical analysis was done using Welch's two-sample t-test and statistical significance defined as $p \leq 0.05$.

Analysis of mitochondrial membrane potential (Δψm)

Quantitative analysis of Δψm was performed by flow cytometry. Cells were grown in pluripotency or differentiating conditions, as described above. Cells were dissociated and pelleted to obtain 2E05 cells per sample for the staining procedure.

For TMRM staining in single cells from early mouse epiblasts, embryos were dissected at E5.5 and cultured overnight in the presence or absence of caspase inhibitors. On the following morning, to avoid misleading readings, epiblasts were isolated initially by an enzymatic treatment with of 2.5% pancreatin, 0.5% trypsin and 0.5% polyvinylpyrrolidone (PVP40) - all from Sigma-Aldrich- to remove the visceral endoderm (VE). Embryos were treated during 8 min at 4ºC, followed by 2 min at RT. The VE was then pealed with the forceps and the extraembryonic ectoderm removed to isolate the epiblasts. Up to 16 epiblasts were pooled per 600µL of Accutase (Sigma-Aldrich) for dissociation into single cells prior to staining. Reaction was stopped with equal volume of FCS and cells subjected to TMRM staining.

Cells were loaded with 10 nM of the Nernstian probe tetramethylrhodamin methyl ester perchlorate (TMRM, Sigma), prepared in N2B27 media. After incubating for 15 min at 37ºC, cells were pelleted again and re-suspended in flow cytometry (FC) buffer (3% FCS in DPBS). Sytox blue (1:1000, Invitrogen, UK) was used as viability staining. Stained cell suspensions were analysed in BD LSRII flow cytometer operated through FACSDiva software (Becton Dickinson Biosciences, UK). For TMRM fluorescence detection the yellow laser was adjusted for excitation at λ=562 nm, capturing the emission light at λ=585 nm for TMRM (Floryk and Houštěk, 1999; Scaduto and Grotyohann, 1999). In the case of GFP-labelled cell lines, for GFP fluorescence detection the blue laser was adjusted for excitation at λ=488 nm, capturing the emission light at λ=525 nm. Results were analysed in FlowJo vX10.0.7r2.

Qualitative analysis of Δψm was performed by confocal microscopy. Wild-type and *Bmpr1a*$^{-/-}$ cells were grown in fibronectin-coated glass coverslips. At the third day of differentiation, cells were loaded with 200 nM MitoTracker Red probe (Life Technologies), prepared in N2B27 media, for 15 min at 37ºC. Cells were then washed with DPBS and fixed with 3.7% formaldehyde for subsequent immunocytochemical staining of total mitochondria mass, with TOMM20 antibody.

Immunofluorescence

Cells were washed with DPBS and fixed with 3.7% formaldehyde (Sigma, UK) in N2B27, for 15 min at 37ºC. Permeabilization of the cell membranes was done with 0.4% Triton X-100 in DPBS (DPBS-Tx), at RT with agitation. Blocking step with 5% BSA in DPBS-Tx 0.1% was performed for

30 min, at RT with agitation. Mitochondria were labelled with TOMM20 antibody (1:100, Santa Cruz Biotechnologies). Dead cells were labelled with cleaved caspase-3 antibody (1:400, CST) and NANOG antibody was used to mark pluripotent cells (1:100, eBioscience). Secondary antibodies were Alexa Fluor (1:600, Invitrogen). Primary antibody incubation was performed overnight at 4ºC and secondary antibody incubation during 45 min, together with Hoechst to stain nuclei (1:1000, ThermoScientific), at RT and protected from light. In both cases antibodies were diluted in blocking solution. Three 10 min washes with DPBS-Tx 0.1% were performed between each critical step and before mounting with Vectashield medium (Vector Laboratories).

Samples were imaged with a Zeiss LSM780 confocal microscope (Zeiss, UK) and processed with Fiji software (Schindelin et al., 2012). Mitochondria stainings were imaged with a 63x/1.4 Oil objective. For samples stained with TOMM20 antibody and MitoTracker Red, Z-stacks were acquired and processed for deconvolution using Huygens software (Scientific Volume Imaging, https://svi.nl/). Samples stained with cleaved caspase-3 were imaged with 20x/0.8 magnification objective. Imaging and deconvolution analysis were performed with the support and advice from Mr. Stephen Rothery from the Facility for Imaging by Light Microscopy (FILM) at Imperial College London.

Embryo immunofluorescent staining for p-rpS6, OPA1 and DDIT3 (CHOP) markers was performed as follows. Cultured embryos were fixed in 4% PFA in DPBS containing 0.01% Triton and 0.1% Tween 20 during 20 min at RT. Permeabilization of the membranes was done during 10 min in DPBS with 0.5% Triton. Embryos were blocked in 5% BSA in DPBS with 0.25% Triton during 45 min. Incubation with primary antibodies - CHOP (1:500, CST), OPA1 (1:100, BD Biosciences) and p-rpS6 (CST, UK) - was done overnight at 4ºC in 2.5% BSA in DPBS with 0.125% Triton. On the following morning, hybridisation with secondary antibodies Alexa Fluor 568 and Alexa Fluor 488 (diluted 1:600 in DPBS with 2.5% BSA and 0.125% Triton) was done next during 1h at RT. Hoechst was also added to this mixture to stain nuclei (1:1000). Three 10 min washes with filtered DPBS-Tx 0.1% were performed between each critical step. All steps were done with gentle agitation.

Embryos were imaged in embryo dishes (Nunc) in a drop of Vectashield using Zeiss LSM780 confocal microscope at 40x magnification.

Western Blotting

Cells were washed in DPBS and lysed with Laemmli lysis buffer (0.05 M Tris- HCl at pH 6.8, 1% SDS, 10% glycerol, 0.1% β-mercaptoethanol in distilled water). Total protein quantification was done using BCA assay (Thermo Scientific, UK) and samples (15µg of protein per lane) were loaded into 12% Bis-Tris protein gels (BioRad). Resolved proteins were transferred into nitrocellulose membranes (GE Healthcare). The following primary antibodies were incubated

overnight at 4ºC: rabbit anti-TOMM20 (1:1000, CST-42406), rabbit anti-α-Tubulin (1:1000, CST-2144), mouse anti-mt-CO1 (1:2000, ab14705), rabbit anti-DRP1 (1:1000, CST- 8570), mouse anti-MFN1 (ab57602), mouse anti-MFN2 (ab56889) and mouse anti-Vinculin (1:1000, Sigma V9131). On the following morning, HRP-conjugated secondary antibodies (Santa Cruz) were incubated for 1h at RT. Membranes were developed with ECL reagents (Promega) and mounted in cassette for time-time-controlled exposure to film (GE Healthcare).

Bulk RNA-Seq and Single cell RNA-Seq

For bulk RNA Seq in the competitive scenario between cells with different mtDNA, HB(24%) and BG(95%) mESCs were grown separately or in co-culture. On the third day of culture cells were dissociated and subjected to fluorescence activated cell sorting (FACS) to separate the cell populations in co-culture. To control for eventual transcriptional changes due to the FACS process, a mixture of the two separate populations was subjected to the same procedure as the co-cultured samples. Total RNA isolation was then carried out using RNA extraction Kit (RNeasy Mini Kit, Qiagen). PolyA selection/enrichment was the method adopted for library preparation, using the NEB Ultra II RNA Prep Kit. Single end 50bp libraries were sequenced on Illumina Hiseq 2500. Raw basecall files were converted to fastq files using Illumina's bcl2fastq (version 2.1.7). Reads were aligned to mouse genome (mm9) using Tophat2 version 2.0.11 (Kim et al., 2013) with default parameters. Mapped reads that fell on genes were counted using featureCounts from Rsubread package (Liao et al., 2019). Generated count data were then used to identify differentially expressed genes using DESeq2 (Love et al., 2014). Genes with very low read counts were excluded. Finally, Gene Set Enrichment Analysis was performed using GSEA software (Mootha et al., 2003; Subramanian et al., 2005) on pre-ranked list generated by DESeq2.

To investigate the nature of cells eliminated by cell competition during early mouse embryogenesis by means of Single Cell RNA-Sequencing (scRNA-seq), early mouse embryos were dissected at E5.5 and cultured overnight in the presence or absence of caspase inhibitors. On the following morning, embryos were dissociated with Accutase and subjected to single-cell sorting into 384-well plate. Total RNA isolation was then carried out using a RNA extraction Kit (RNeasy Mini Kit, Qiagen). scRNA-seq was performed using the Smart-Seq2 illumina method. PolyA selection/enrichment with Ultra II Kit (NEB) was the method adopted for library preparation.

Data processing, quality control and normalization

We performed transcript quantification in our scRNA-seq data by running Salmon v0.8.2 (Patro et al., 2017) in the quasi-mapping-based mode. First, a transcriptome index was created from the mouse reference (version GRCm38.p4) and ERCC spike-in sequences. Then, the quantification step was carried out with the "quant" function, correcting for the sequence-specific biases ("--seqBias" flag) and the fragment-level GC biases ("--gcBias" flag). Finally, the transcript level

abundances were aggregated to gene level counts. On the resulting raw count matrix including 1,495 cells, we apply a quality control to exclude poor quality cells from downstream analyses. For the quality control we used the following criteria: we identified the cells that have a log10 total number of reads equal to or greater than 4, a fraction of mapped reads equal to or greater than 0.8, a number of genes with expression level above 10 reads per million equal to or greater than 3000 and a fraction of reads mapped to endogenous genes equal to or greater than 0.5. This resulted in the selection of 723 cells, which were kept for downstream analyses. Transcripts per million (TPM) normalization (as estimated by Salmon) was used.

Identification of highly variable genes and dimensionality reduction

To identify highly variable genes (HVG), first we fitted a mean-total variance trend using the R function "trendVar" and then the variance was decomposed into biological and technical components with the R function "decomposeVar"; both functions are included in the package "scran" (version 1.6.9 (Lun et al., 2016)).

We considered HVGs those that have a biological component that is significantly greater than zero at a false discovery rate (Benjamini-Hochberg method) of 0.05. Then, we applied further filtering steps by keeping only genes that have an average expression greater to or equal than 10 TPM and are significantly correlated with one another (function "correlatePairs" in "scran" package, FDR<0.05). This yielded 1921 genes, which were used to calculate a distance matrix between cells defined as $\sqrt{(1-\rho)/2}$, where ρ is the Spearman's correlation coefficient between cells. A 2D representation of the data was obtained with UMAP package (version 0.2.0.0 https://cran.r-project.org/web/packages/umap/index.html) using the distance matrix as input.

Cell clustering

To classify cells into different clusters, we ran hierarchical clustering on the distance matrix (see above; "hclust" function in R with ward.D2 aggregation method) followed by the dynamic hybrid cut algorithm ("cutreeDynamic" function in R package "dynamicTreeCut" (https://CRAN.R-project.org/package=dynamicTreeCut) version 1.63.1, with the hybrid method, a minimum cluster size of 35 cells and a "deepSplit" parameter equal to 0), which identified five clusters. Cells from different batches were well mixed across these five clusters (see Figure S1), suggesting that the batch effect was negligible.

Identification of a single-cell trajectory in the epiblast

We calculated a diffusion map ("DiffusionMap" function in the R package "destiny" version 2.6.2 (Angerer et al., 2016) on the distance defined above on the epiblast cells from CI-treated embryos. The pseudotime coordinate was computed with the "DPT" function with the root cell in the winner epiblast cluster (identified by the function "tips" in the "destiny" package). Such pseudotime

coordinate can be interpreted as a "losing score" for all the epiblast cells from the CI-treated embryos.

We estimated the losing scores of the epiblast cells from DMSO-treated embryos by projecting such data onto the diffusion map previously calculated (function "dm_predict" in the destiny package). Finally, for each of the projected cells, we assigned the losing score as the average of the losing scores of the 10 closest neighbours in the original diffusion map (detected with the function "projection-dist" in the destiny package).

Differential gene expression analysis along the trajectory

To identify the genes that are differentially expressed along the trajectory, first we kept only genes that have more than 15 TPM in more than 10 cells (this list of genes is provided in Supplementary Table 4); then, we obtained the log-transformed expression levels of these genes (adding 1 as a pseudo-count to avoid infinities) as a function of the losing score and we fitted a generalized additive model to them (R function "gam" from "GAM" package version 1.16.). We used the ANOVA test for parametric effect provided by the gam function to estimate a p-value for each tested gene. This yielded a list of 5,311 differentially expressed genes (FDR < 0.01).

Next, we looked for groups of differentially expressed genes that share similar expression patterns along the trajectory. To this aim, similarly to what we did when clustering cells, we calculated a correlation-based distance matrix between genes, defined as $\sqrt{(1-\rho)/2}$, where ρ is the Spearman's correlation coefficient between genes. Hierarchical clustering was then applied to this matrix (hclust function in R, with ward.D2 method) followed by the dynamic hybrid cut algorithm (dynamicTreeCut package) to define clusters ("cutreeDynamic" function in R with the hybrid method and a minimum cluster size of 100 genes and a deepSplit parameter equal to 0). This resulted in the definition of four clusters, three of genes that decrease along the trajectory (merged together for the GO enrichment and the IPA analysis) and one of increasing genes (Figure S2D). IPA (QIAGEN Inc., https://www.qiagenbio- informatics.com/products/ingenuity-pathway-analysis), was run on all genes differentially expressed (FDR < 0.01) along the trajectory from winner to loser cells (see Figures 2A-D and Figures 3A-C), using all the tested genes as a background (see Supplementary Table 4). This software generated networks, canonical pathways and functional analysis. The list of decreasing/increasing genes is provided in Supplementary Tables 1 and 2.

Analysis of Mitochondrial DNA heteroplasmy

We used STAR (version 2.7 (Dobin et al., 2013)) to align the transcriptome of the epiblast cells from CI-treated embryos (274) to the mouse reference genome (mm10). Only reads that uniquely mapped to the mitochondrial DNA (mtDNA) were considered. From these, we obtained allele counts at each mtDNA position with a Phred Quality Score greater than 33 using the samtools mpileup function.

Next, we applied filters to remove cells and mtDNA positions with a low coverage. First, we removed cells with fewer than 2,000 mtDNA positions covered by more than 50 reads. Second, we removed positions having less than 50 reads in more than 50% of cells in each of the three epiblast clusters (winner, intermediate and loser). These two filters resulted in 259 cells and 5,192 mtDNA positions being considered for further analyses.

Starting from these cells and positions, we applied an additional filter to keep only positions with a sufficiently high level of heteroplasmy. To this aim, for each position with more than 50 reads in a cell, we estimated the heteroplasmy as:

$$H = 1 - f_{max}$$

where f_{max} is the frequency of the most common allele. We kept only positions with H>0.01 in at least 10 cells.

Finally, using generalized additive models (see above), we identified the positions whose heteroplasmy H changes as a function of the cells' losing score in a statistically significant way. We found a total of eleven significant positions (FDR < 0.001), six of them in the *mt-Rnr1* gene and five in the *mt-Rnr2* gene. All of these positions have a higher level of heteroplasmy in loser cells (see Figure 6B-G and Figure S5F-K). The results remain substantially unaltered if the Spearman's rank correlation test (in alternative to the generalized additive models) is used.

For the barplot shown in Figure 6H and the correlation heatmaps in Figure 6I and S5L, we took into account only cells that covered with more than 50 reads all the significant positions in the *mt-Rnr1* gene (215 cells, Figures 6H and 6I) or in both the *mt-Rnr1* and *mt-Rnr2* genes (214 cells, Figure S5L).

As a negative control, we repeated the analysis described above using the ERCC spike-ins added to each cell. As expected, none of the positions was statistically significant, which suggested that our procedure is robust against sequence errors introduced during PCR amplification.

Common features of scRNA-seq and bulk RNA-seq datasets

Differential expression analysis between the co-cultured winner HB(24%) and loser cell line BG(95%) was performed using the package EdgeR version 3.20.9 (Robinson et al., 2010).

Batches were specified in the argument of the function model.matrix. We fitted a quasi-likelihood negative binomial generalized log-linear model (with the function glmQLFit) to the genes that were filtered by the function filterByExpr (with default parameter). These genes were used as background for the gene enrichment analysis.

We set a FDR of 0.001 as a threshold for significance. The enrichment analysis for both the scRNA-seq and bulk RNA-seq datasets were performed using the tool g:Profiler (Reimand et al., 2011). The list of up-regulated, down-regulated and background genes related to the DE analysis for the bulk RNA-seq dataset are provided in the Supplementary Tables 5, 6 and 7.

Quantification and Statistical Analysis

Flow cytometry data was analysed with FlowJo Software.

Western blot quantification was performed using Image Studio Lite (LI-COR). Protein expression levels were normalised to loading controls vinculin or α-tubulin.

The quantification of the DDIT3 and OPA1 expression in embryos was done by two distinct methods. DDIT3 expression was quantified by counting the number of epiblast cells with positive staining in the embryos of each group. The expression of OPA1 was quantified on Fiji software as the mean fluorescence across a 10 pixel width line drawn on the basal cytoplasm of each cell with high or low p-rpS6 fluorescence intensity, as specified in (Bowling *et al.*, 2018). A min of 8 cells were quantified per condition (high vs low mTOR activity) in each embryo. Six embryos treated with CI were analysed. Mean grey values of OPA1 fluorescence for each epiblast cell are pooled on the same graph.

The statistical analysis of the results was performed using GraphPad Prism v8 Software (GraphPad Software, United States of America). Data was tested for normality using Shapiro-Wilk normality test. Parametric or non-parametric statistical tests were applied accordingly. Details about the test used in each of the experiments are specified in figure legends. Statistical significance was considered with a confidence interval of 0.05%. n.s., non-significant; * $p<0.05$; ** $p<0.01$;*** $p<0.001$.

Data and Code Availability

Data were analysed with standard programs and packages, as detailed above. Code is available on request. Raw as well as processed data are available through ArrayExpress, accession numbers E-MTAB-8640, for scRNA-seq data, and E-MTAB-8692, for bulk RNA-seq data.

References

Allio, R., Donega, S., Galtier, N., and Nabholz, B. (2017). Large Variation in the Ratio of Mitochondrial to Nuclear Mutation Rate across Animals: Implications for Genetic Diversity and the Use of Mitochondrial DNA as a Molecular Marker. Mol Biol Evol *34*, 2762-2772.

Angerer, P., Haghverdi, L., Buttner, M., Theis, F.J., Marr, C., and Buettner, F. (2016). destiny: diffusion maps for large-scale single-cell data in R. Bioinformatics *32*, 1241-1243.

Bowling, S., Di Gregorio, A., Sancho, M., Pozzi, S., Aarts, M., Signore, M., M, D.S., Barbera, J.P.M., Gil, J., and Rodriguez, T.A. (2018). P53 and mTOR signalling determine fitness selection through cell competition during early mouse embryonic development. Nat Commun *9*, 1763.

Bowling, S., Lawlor, K., and Rodriguez, T.A. (2019). Cell competition: the winners and losers of fitness selection. Development *146*.

Burgstaller, J.P., Johnston, I.G., Jones, N.S., Albrechtova, J., Kolbe, T., Vogl, C., Futschik, A., Mayrhofer, C., Klein, D., Sabitzer, S.*, et al.* (2014). MtDNA segregation in heteroplasmic tissues is common in vivo and modulated by haplotype differences and developmental stage. Cell Rep *7*, 2031-2041.

Burgstaller, J.P., Johnston, I.G., and Poulton, J. (2015). Mitochondrial DNA disease and developmental implications for reproductive strategies. Mol Hum Reprod *21*, 11-22.

Burr, S.P., Pezet, M., and Chinnery, P.F. (2018). Mitochondrial DNA Heteroplasmy and Purifying Selection in the Mammalian Female Germ Line. Dev Growth Differ *60*, 21-32.

Chen, H., Detmer, S.A., Ewald, A.J., Griffin, E.E., Fraser, S.E., and Chan, D.C. (2003). Mitofusins Mfn1 and Mfn2 coordinately regulate mitochondrial fusion and are essential for embryonic development. J Cell Biol *160*, 189-200.

Chinnery, P.F., and Hudson, G. (2013). Mitochondrial genetics. Br Med Bull *106*, 135-159.

Claveria, C., Giovinazzo, G., Sierra, R., and Torres, M. (2013). Myc-driven endogenous cell competition in the early mammalian embryo. Nature *500*, 39-44.

Czechanski, A., Byers, C., Greenstein, I., Schrode, N., Donahue, L.R., Hadjantonakis, A.K., and Reinholdt, L.G. (2014). Derivation and characterization of mouse embryonic stem cells from permissive and nonpermissive strains. Nat Protoc *9*, 559-574.

Di-Gregorio, A., Sancho, M., Stuckey, D.W., Crompton, L.A., Godwin, J., Mishina, Y., and Rodriguez, T.A. (2007). BMP signalling inhibits premature neural differentiation in the mouse embryo. Development *134*, 3359-3369.

Diaz-Diaz, C., Fernandez de Manuel, L., Jimenez-Carretero, D., Montoya, M.C., Claveria, C., and Torres, M. (2017). Pluripotency Surveillance by Myc-Driven Competitive Elimination of Differentiating Cells. Dev Cell *42*, 585-599 e584.

Diaz-Diaz, C., and Torres, M. (2019). Insights into the quantitative and dynamic aspects of Cell Competition. Curr Opin Cell Biol *60*, 68-74.

Dobin, A., Davis, C.A., Schlesinger, F., Drenkow, J., Zaleski, C., Jha, S., Batut, P., Chaisson, M., and Gingeras, T.R. (2013). STAR: ultrafast universal RNA-seq aligner. Bioinformatics *29*, 15-21.

Ellis, S.J., Gomez, N.C., Levorse, J., Mertz, A.F., Ge, Y., and Fuchs, E. (2019). Distinct modes of cell competition shape mammalian tissue morphogenesis. Nature *569*, 497-502.

Fan, W., Waymire, K.G., Narula, N., Li, P., Rocher, C., Coskun, P.E., Vannan, M.A., Narula, J., Macgregor, G.R., and Wallace, D.C. (2008). A mouse model of mitochondrial disease reveals germline selection against severe mtDNA mutations. Science *319*, 958-962.

Fischer, M. (2017). Census and evaluation of p53 target genes. Oncogene *36*, 3943-3956.

Floros, V.I., Pyle, A., Dietmann, S., Wei, W., Tang, W.C.W., Irie, N., Payne, B., Capalbo, A., Noli, L., Coxhead, J.*, et al.* (2018). Segregation of mitochondrial DNA heteroplasmy through a developmental genetic bottleneck in human embryos. Nat Cell Biol *20*, 144-151.

Freyer, C., Cree, L.M., Mourier, A., Stewart, J.B., Koolmeister, C., Milenkovic, D., Wai, T., Floros, V.I., Hagstrom, E., Chatzidaki, E.E.*, et al.* (2012). Variation in germline mtDNA heteroplasmy is determined prenatally but modified during subsequent transmission. Nat Genet *44*, 1282-1285.

Gorman, G.S., Chinnery, P.F., DiMauro, S., Hirano, M., Koga, Y., McFarland, R., Suomalainen, A., Thorburn, D.R., Zeviani, M., and Turnbull, D.M. (2016). Mitochondrial diseases. Nat Rev Dis Primers *2*, 16080.

Haghverdi, L., Buttner, M., Wolf, F.A., Buettner, F., and Theis, F.J. (2016). Diffusion pseudotime robustly reconstructs lineage branching. Nature methods *13*, 845-848.

Hashimoto, M., and Sasaki, H. (2019). Epiblast Formation by TEAD-YAP-Dependent Expression of Pluripotency Factors and Competitive Elimination of Unspecified Cells. Dev Cell *50*, 139-154 e135.

Johnston, I.G., Burgstaller, J.P., Havlicek, V., Kolbe, T., Rulicke, T., Brem, G., Poulton, J., and Jones, N.S. (2015). Stochastic modelling, Bayesian inference, and new in vivo measurements elucidate the debated mtDNA bottleneck mechanism. Elife *4*, e07464.

Kauppila, J.H.K., Baines, H.L., Bratic, A., Simard, M.L., Freyer, C., Mourier, A., Stamp, C., Filograna, R., Larsson, N.G., Greaves, L.C.*, et al.* (2016). A Phenotype-Driven Approach to Generate Mouse Models with Pathogenic mtDNA Mutations Causing Mitochondrial Disease. Cell Rep *16*, 2980-2990.

Khrapko, K., Coller, H.A., Andre, P.C., Li, X.C., Hanekamp, J.S., and Thilly, W.G. (1997). Mitochondrial mutational spectra in human cells and tissues. Proc Natl Acad Sci U S A *94*, 13798-13803.

Kim, D., Pertea, G., Trapnell, C., Pimentel, H., Kelley, R., and Salzberg, S.L. (2013). TopHat2: accurate alignment of transcriptomes in the presence of insertions, deletions and gene fusions. Genome Biol *14*, R36.

Kojima, Y., Kaufman-Francis, K., Studdert, J.B., Steiner, K.A., Power, M.D., Loebel, D.A., Jones, V., Hor, A., de Alencastro, G., Logan, G.J.*, et al.* (2014). The transcriptional and functional properties of mouse epiblast stem cells resemble the anterior primitive streak. Cell Stem Cell *14*, 107-120.

Kon, S., Ishibashi, K., Katoh, H., Kitamoto, S., Shirai, T., Tanaka, S., Kajita, M., Ishikawa, S., Yamauchi, H., Yako, Y.*, et al.* (2017). Cell competition with normal epithelial cells promotes apical extrusion of transformed cells through metabolic changes. Nat Cell Biol *19*, 530-541.

Kramer, A., Green, J., Pollard, J., Jr., and Tugendreich, S. (2014). Causal analysis approaches in Ingenuity Pathway Analysis. Bioinformatics *30*, 523-530.

Kucinski, I., Dinan, M., Kolahgar, G., and Piddini, E. (2017). Chronic activation of JNK JAK/STAT and oxidative stress signalling causes the loser cell status. Nat Commun *8*, 136.

Latorre-Pellicer, A., Lechuga-Vieco, A.V., Johnston, I.G., Hamalainen, R.H., Pellico, J., Justo-Mendez, R., Fernandez-Toro, J.M., Claveria, C., Guaras, A., Sierra, R.*, et al.* (2019). Regulation of Mother-to-Offspring Transmission of mtDNA Heteroplasmy. Cell Metab.

Lee, H.S., Ma, H., Juanes, R.C., Tachibana, M., Sparman, M., Woodward, J., Ramsey, C., Xu, J., Kang, E.J., Amato, P.*, et al.* (2012). Rapid mitochondrial DNA segregation in primate preimplantation embryos precedes somatic and germline bottleneck. Cell Rep *1*, 506-515.

Liao, Y., Smyth, G.K., and Shi, W. (2019). The R package Rsubread is easier, faster, cheaper and better for alignment and quantification of RNA sequencing reads. Nucleic Acids Res *47*, e47.

Lima, A., Burgstaller, J., Sanchez-Nieto, J.M., and Rodriguez, T.A. (2018). The Mitochondria and the Regulation of Cell Fitness During Early Mammalian Development. Curr Top Dev Biol *128*, 339-363.

Love, M.I., Huber, W., and Anders, S. (2014). Moderated estimation of fold change and dispersion for RNA-seq data with DESeq2. Genome Biol *15*, 550.

Ludwig, L.S., Lareau, C.A., Ulirsch, J.C., Christian, E., Muus, C., Li, L.H., Pelka, K., Ge, W., Oren, Y., Brack, A.*, et al.* (2019). Lineage Tracing in Humans Enabled by Mitochondrial Mutations and Single-Cell Genomics. Cell *176*, 1325-1339 e1322.

Lun, A.T., McCarthy, D.J., and Marioni, J.C. (2016). A step-by-step workflow for low-level analysis of single-cell RNA-seq data with Bioconductor. F1000Res *5*, 2122.

Madan, E., Gogna, R., and Moreno, E. (2018). Cell competition in development: information from flies and vertebrates. Curr Opin Cell Biol *55*, 150-157.

Melber, A., and Haynes, C.M. (2018). UPR(mt) regulation and output: a stress response mediated by mitochondrial-nuclear communication. Cell Res *28*, 281-295.

Mootha, V.K., Lindgren, C.M., Eriksson, K.F., Subramanian, A., Sihag, S., Lehar, J., Puigserver, P., Carlsson, E., Ridderstrale, M., Laurila, E.*, et al.* (2003). PGC-1alpha-responsive genes

involved in oxidative phosphorylation are coordinately downregulated in human diabetes. Nat Genet *34*, 267-273.
Morata, G., and Ripoll, P. (1975). Minutes: mutants of drosophila autonomously affecting cell division rate. Dev Biol *42*, 211-221.
Mouchiroud, L., Houtkooper, R.H., Moullan, N., Katsyuba, E., Ryu, D., Canto, C., Mottis, A., Jo, Y.S., Viswanathan, M., Schoonjans, K.*, et al.* (2013). The NAD(+)/Sirtuin Pathway Modulates Longevity through Activation of Mitochondrial UPR and FOXO Signaling. Cell *154*, 430-441.
Munch, C. (2018). The different axes of the mammalian mitochondrial unfolded protein response. BMC Biol *16*, 81.
Nargund, A.M., Pellegrino, M.W., Fiorese, C.J., Baker, B.M., and Haynes, C.M. (2012). Mitochondrial import efficiency of ATFS-1 regulates mitochondrial UPR activation. Science *337*, 587-590.
Patro, R., Duggal, G., Love, M.I., Irizarry, R.A., and Kingsford, C. (2017). Salmon provides fast and bias-aware quantification of transcript expression. Nat Methods *14*, 417-419.
Prudent, J., and McBride, H.M. (2017). The mitochondria-endoplasmic reticulum contact sites: a signalling platform for cell death. Curr Opin Cell Biol *47*, 52-63.
Quiros, P.M., Mottis, A., and Auwerx, J. (2016). Mitonuclear communication in homeostasis and stress. Nat Rev Mol Cell Biol *17*, 213-226.
Quiros, P.M., Prado, M.A., Zamboni, N., D'Amico, D., Williams, R.W., Finley, D., Gygi, S.P., and Auwerx, J. (2017). Multi-omics analysis identifies ATF4 as a key regulator of the mitochondrial stress response in mammals. J Cell Biol *216*, 2027-2045.
Rajasimha, H.K., Chinnery, P.F., and Samuels, D.C. (2008). Selection against pathogenic mtDNA mutations in a stem cell population leads to the loss of the 3243A-->G mutation in blood. Am J Hum Genet *82*, 333-343.
Ran, F.A., Hsu, P.D., Wright, J., Agarwala, V., Scott, D.A., and Zhang, F. (2013). Genome engineering using the CRISPR-Cas9 system. Nat Protoc *8*, 2281-2308.
Reimand, J., Arak, T., and Vilo, J. (2011). g:Profiler--a web server for functional interpretation of gene lists (2011 update). Nucleic Acids Res *39*, W307-315.
Robinson, M.D., McCarthy, D.J., and Smyth, G.K. (2010). edgeR: a Bioconductor package for differential expression analysis of digital gene expression data. Bioinformatics *26*, 139-140.
Sancho, M., Di-Gregorio, A., George, N., Pozzi, S., Sanchez, J.M., Pernaute, B., and Rodriguez, T.A. (2013). Competitive interactions eliminate unfit embryonic stem cells at the onset of differentiation. Dev Cell *26*, 19-30.
Saveljeva, S., Cleary, P., Mnich, K., Ayo, A., Pakos-Zebrucka, K., Patterson, J.B., Logue, S.E., and Samali, A. (2016). Endoplasmic reticulum stress-mediated induction of SESTRIN 2 potentiates cell survival. Oncotarget *7*, 12254-12266.
Schindelin, J., Arganda-Carreras, I., Frise, E., Kaynig, V., Longair, M., Pietzsch, T., Preibisch, S., Rueden, C., Saalfeld, S., Schmid, B.*, et al.* (2012). Fiji: an open-source platform for biological-image analysis. Nat Methods *9*, 676-682.
Sharpley, M.S., Marciniak, C., Eckel-Mahan, K., McManus, M., Crimi, M., Waymire, K., Lin, C.S., Masubuchi, S., Friend, N., Koike, M.*, et al.* (2012). Heteroplasmy of mouse mtDNA is genetically unstable and results in altered behavior and cognition. Cell *151*, 333-343.
Smirnova, E., Griparic, L., Shurland, D.L., and van der Bliek, A.M. (2001). Dynamin-related protein Drp1 is required for mitochondrial division in mammalian cells. Mol Biol Cell *12*, 2245-2256.
Snow, M.H. (1977). Gastrulation in the mouse: Growth and regionalization of the epiblast. Development *42*, 293-303.
Stewart, J.B., Freyer, C., Elson, J.L., Wredenberg, A., Cansu, Z., Trifunovic, A., and Larsson, N.G. (2008). Strong purifying selection in transmission of mammalian mitochondrial DNA. PLoS Biol *6*, e10.
Stower, M.J., and Srinivas, S. (2018). The Head's Tale: Anterior-Posterior Axis Formation in the Mouse Embryo. Curr Top Dev Biol *128*, 365-390.
Subramanian, A., Tamayo, P., Mootha, V.K., Mukherjee, S., Ebert, B.L., Gillette, M.A., Paulovich, A., Pomeroy, S.L., Golub, T.R., Lander, E.S.*, et al.* (2005). Gene set enrichment

analysis: a knowledge-based approach for interpreting genome-wide expression profiles. Proc Natl Acad Sci U S A *102*, 15545-15550.

Topf, U., Wrobel, L., and Chacinska, A. (2016). Chatty Mitochondria: Keeping Balance in Cellular Protein Homeostasis. Trends Cell Biol *26*, 577-586.

Yun, J., and Finkel, T. (2014). Mitohormesis. Cell Metab *19*, 757-766.

Zhang, H., Burr, S.P., and Chinnery, P.F. (2018). The mitochondrial DNA genetic bottleneck: inheritance and beyond. Essays Biochem *62*, 225-234.

Zhao, Q., Wang, J., Levichkin, I.V., Stasinopoulos, S., Ryan, M.T., and Hoogenraad, N.J. (2002). A mitochondrial specific stress response in mammalian cells. EMBO J *21*, 4411-4419.

Zhou, W., Choi, M., Margineantu, D., Margaretha, L., Hesson, J., Cavanaugh, C., Blau, C.A., Horwitz, M.S., Hockenbery, D., Ware, C.*, et al.* (2012). HIF1alpha induced switch from bivalent to exclusively glycolytic metabolism during ESC-to-EpiSC/hESC transition. EMBO J *31*, 2103-2116.

Graphical Abstract

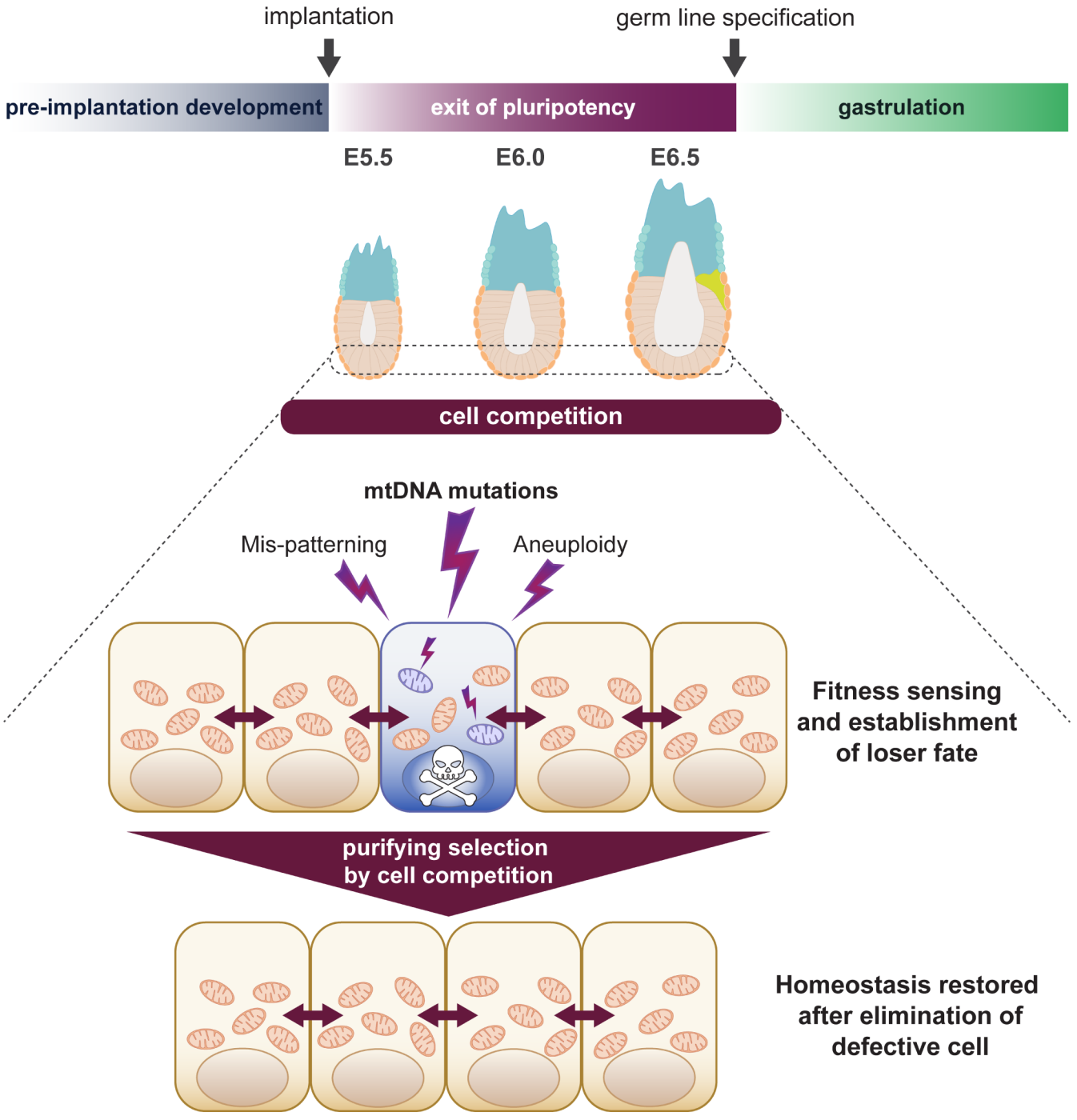

Fig. 1

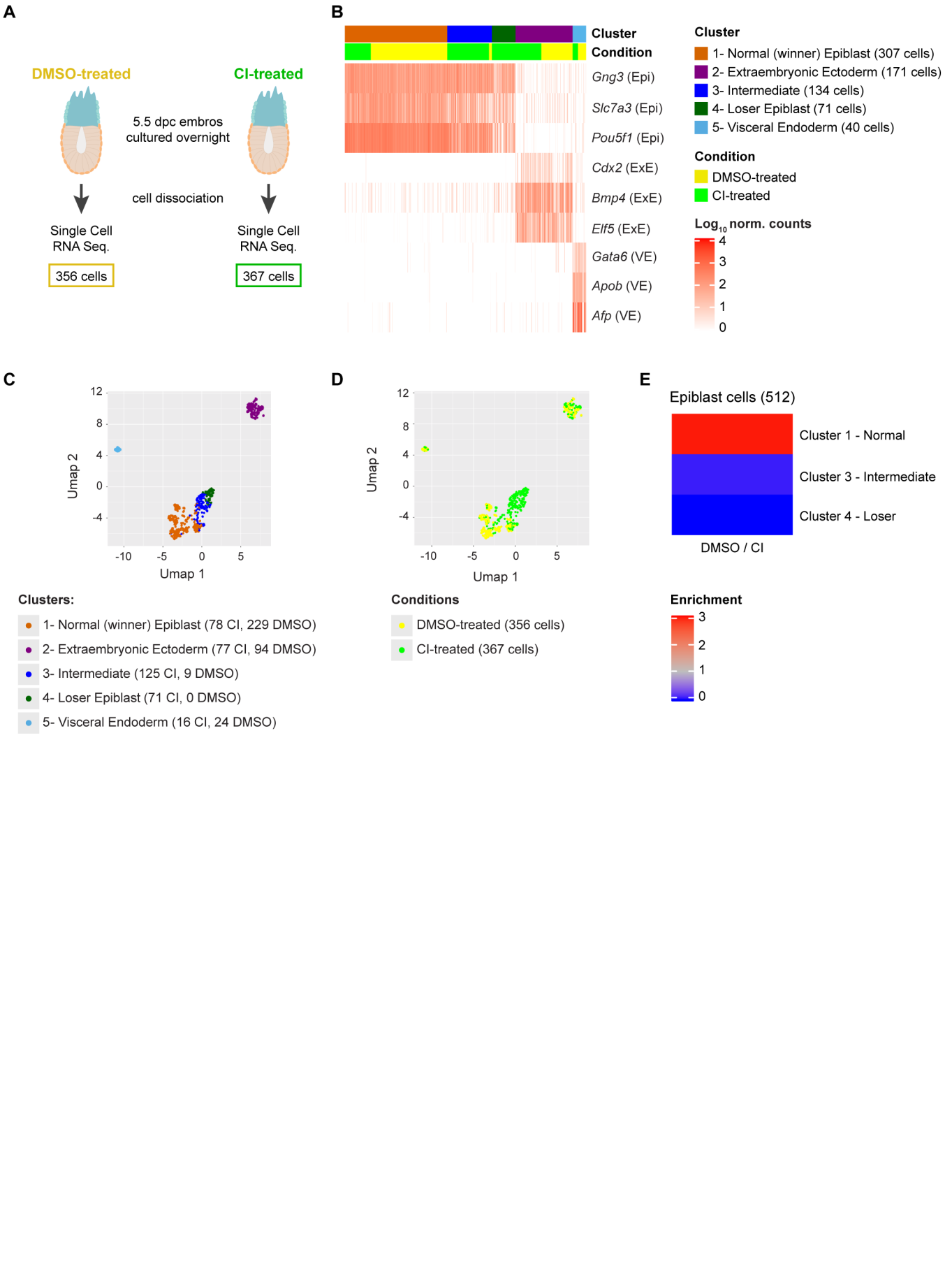
A
DMSO-treated
CI-treated
5.5 dpc embros cultured overnight
cell dissociation
Single Cell RNA Seq.
356 cells
Single Cell RNA Seq.
367 cells
B
Cluster
Condition
Gng3 (Epi)
Slc7a3 (Epi)
Pou5f1 (Epi)
Cdx2 (ExE)
Bmp4 (ExE)
Elf5 (ExE)
Gata6 (VE)
Apob (VE)
Afp (VE)
Cluster
1- Normal (winner) Epiblast (307 cells)
2- Extraembryonic Ectoderm (171 cells)
3- Intermediate (134 cells)
4- Loser Epiblast (71 cells)
5- Visceral Endoderm (40 cells)
Condition
DMSO-treated
CI-treated
Log10 norm. counts
4
3
2
1
0
C
Umap 2
Umap 1
Clusters:
1- Normal (winner) Epiblast (78 CI, 229 DMSO)
2- Extraembryonic Ectoderm (77 CI, 94 DMSO)
3- Intermediate (125 CI, 9 DMSO)
4- Loser Epiblast (71 CI, 0 DMSO)
5- Visceral Endoderm (16 CI, 24 DMSO)
D
Umap 2
Umap 1
Conditions
DMSO-treated (356 cells)
CI-treated (367 cells)
E
Epiblast cells (512)
Cluster 1 - Normal
Cluster 3 - Intermediate
Cluster 4 - Loser
DMSO / CI
Enrichment
3
2
1
0

Fig. 2

A

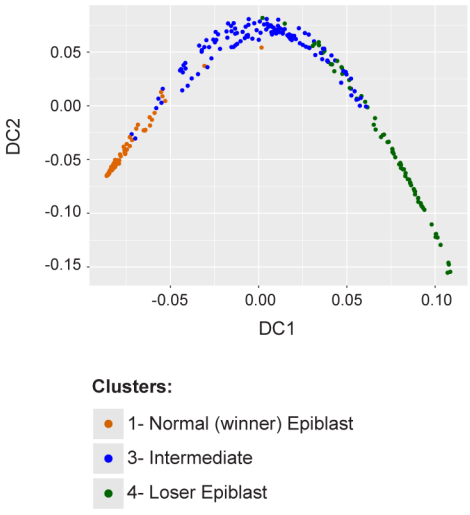

B

Molecular and Cellular Functions	p-value range	# Molecules
Cell Death and Survival	1.90E-02 – 1.32E-14	1181
Protein Synthesis	1.76E-02 – 2.65E-14	743
RNA Damage and Repair	1.59E-06 – 2.44E-12	137
Nucleic Acid Metabolism	1.54E-02 – 2.52E-09	220
Small Molecule Biochemistry	1.84E-02 – 1.20E-08	518

C

Upstream Regulator	Molecule Type	Experimental FDR	p-value of overlap
RICTOR	other	9.3E-04	3.5E-33
TLE3	other	-	1.2E-18
MYC	transcription regulator	-	1.1E-16
MYCN	transcription regulator	2.3E-10	5.6E-16
TP53	transcription regulator	-	3.8E-13
IGF1R	transmembrane receptor	-	1.1E-12
STK11	kinase	-	4.0E-12
NFE2L2	transcription regulator	1.6E-10	7.8E-12
INSR	kinase	-	1.2E-11
LONP1	peptidase	1.1E-06	2.7E-11

D

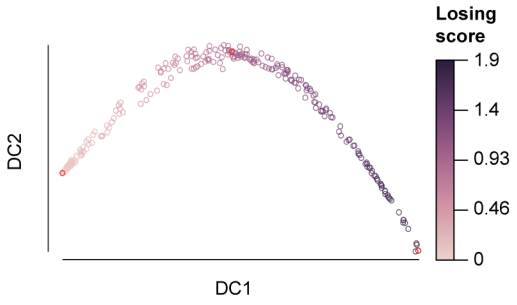

E

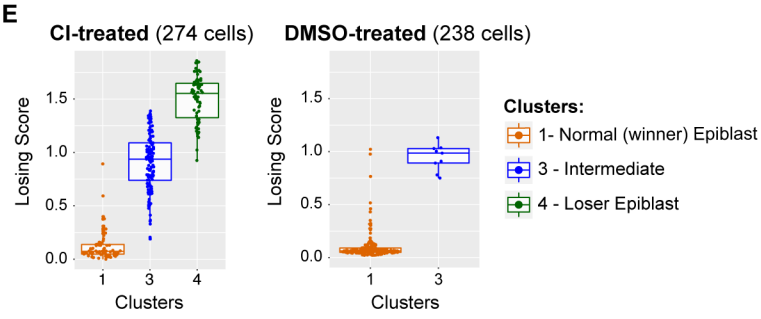

F

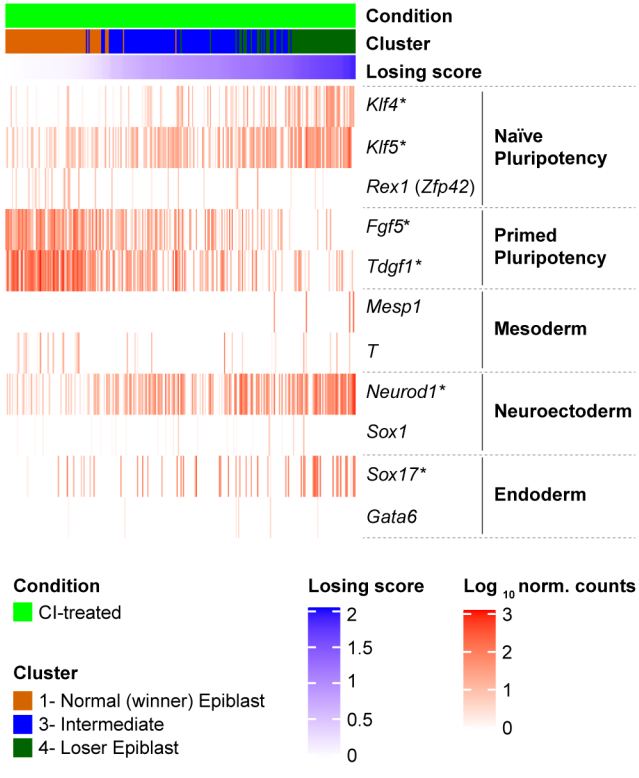

G

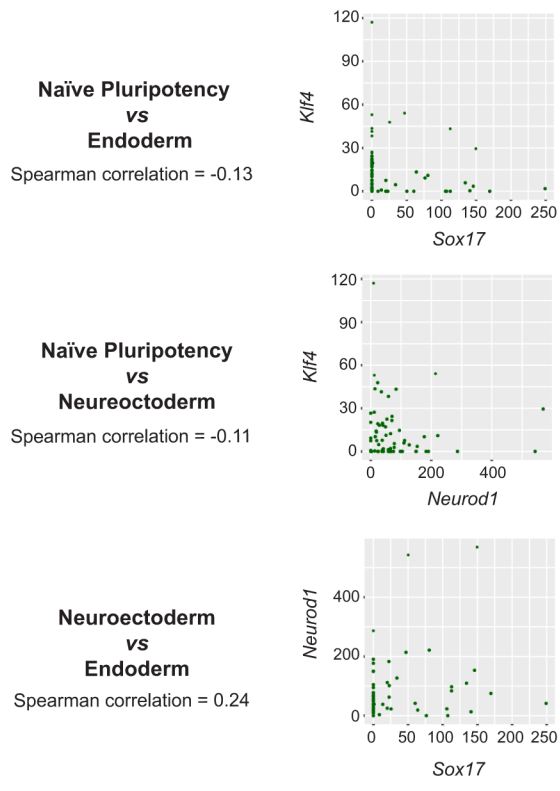

Fig. 3

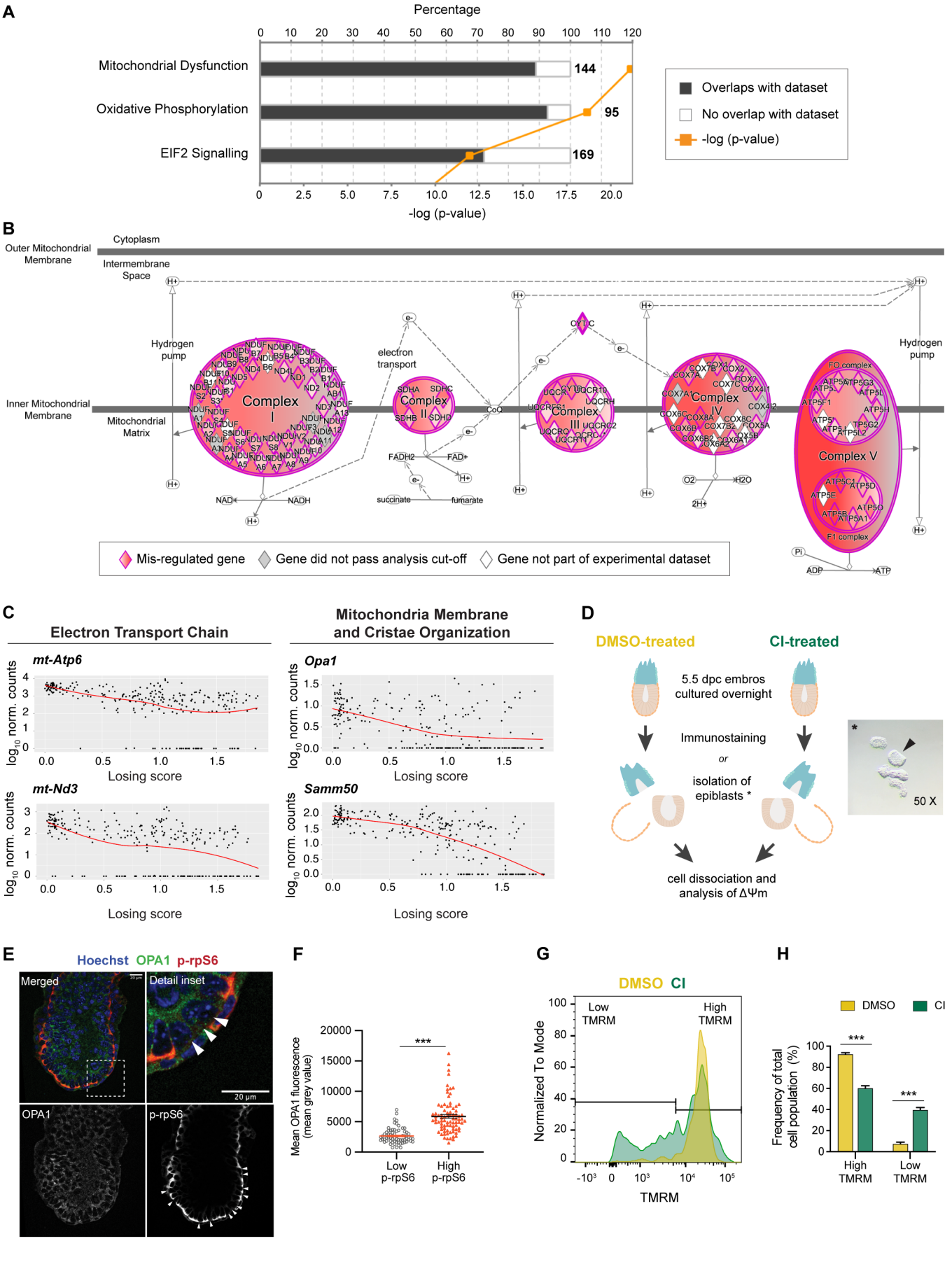
A
Percentage
Mitochondrial Dysfunction
Oxidative Phosphorylation
EIF2 Signalling
144
95
169
Overlaps with dataset
No overlap with dataset
-log (p-value)
-log (p-value)
B
Outer Mitochondrial Membrane
Cytoplasm
Intermembrane Space
Inner Mitochondrial Membrane
Mitochondrial Matrix
Hydrogen pump
electron transport
Complex I
Complex II
Complex III
Complex IV
Complex V
CoQ
CYTC
NAD+
NADH
FADH2
FAD+
succinate
fumarate
O2
H2O
2H+
Pi
ADP
ATP
F1 complex
F0 complex
Mis-regulated gene
Gene did not pass analysis cut-off
Gene not part of experimental dataset
C
Electron Transport Chain
Mitochondria Membrane and Cristae Organization
mt-Atp6
mt-Nd3
Opa1
Samm50
log10 norm. counts
Losing score
D
DMSO-treated
CI-treated
5.5 dpc embros cultured overnight
Immunostaining
or
isolation of epiblasts *
cell dissociation and analysis of ΔΨm
50 X
E
Hoechst OPA1 p-rpS6
Merged
Detail inset
OPA1
p-rpS6
20 µm
F
Mean OPA1 fluorescence (mean grey value)
***
Low p-rpS6
High p-rpS6
G
DMSO CI
Low TMRM
High TMRM
Normalized To Mode
TMRM
H
DMSO
CI
Frequency of total cell population (%)
***
***
High TMRM
Low TMRM

Fig. 4

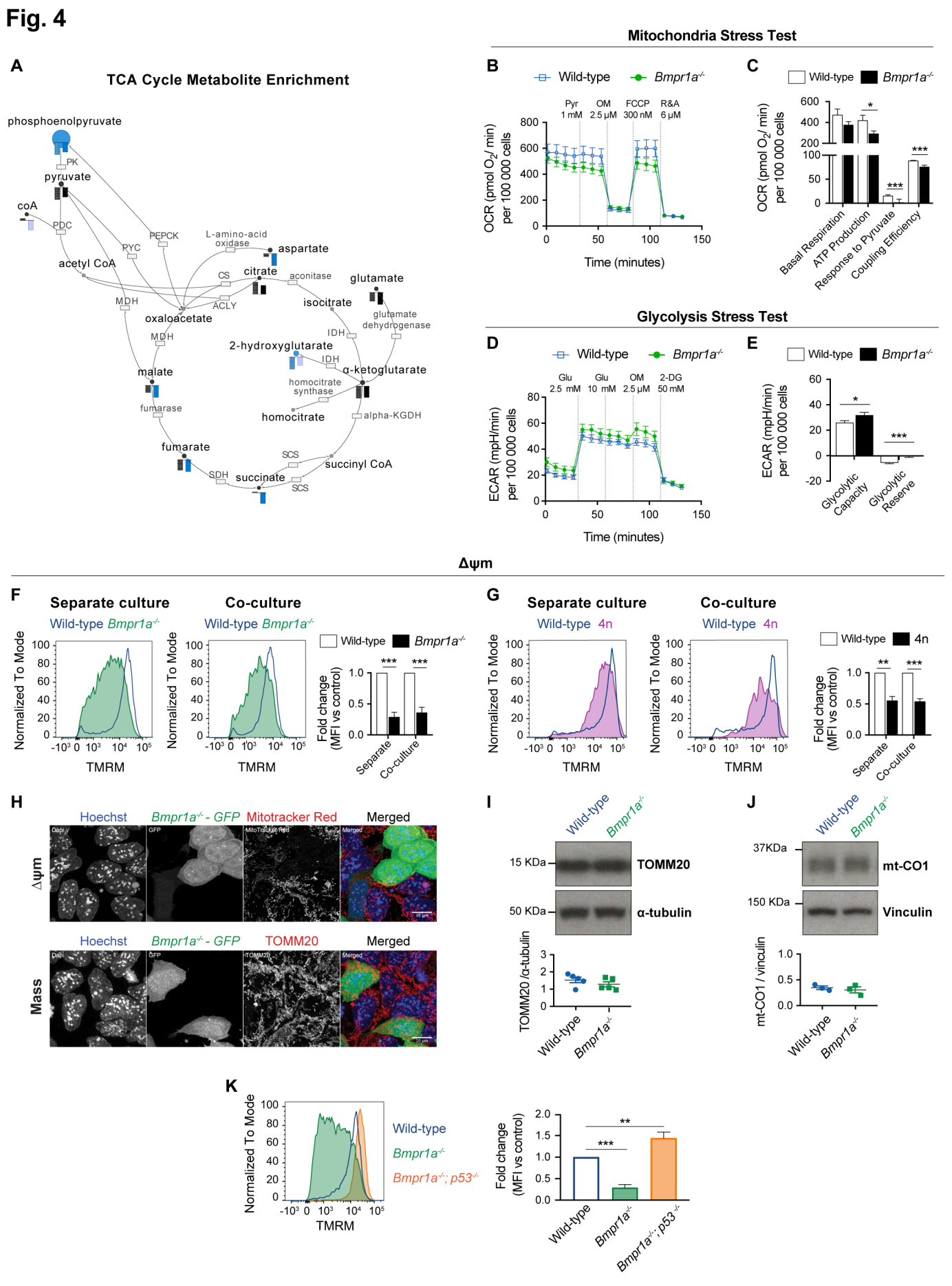
A
TCA Cycle Metabolite Enrichment
phosphoenolpyruvate
PK
pyruvate
coA
PDC
acetyl CoA
PEPCK
PYC
L-amino-acid oxidase
aspartate
CS
citrate
aconitase
glutamate
MDH
ACLY
isocitrate
oxaloacetate
glutamate dehydrogenase
MDH
IDH
2-hydroxyglutarate
IDH
malate
α-ketoglutarate
homocitrate synthase
fumarase
homocitrate
alpha-KGDH
fumarate
SCS
succinyl CoA
SDH
succinate
SCS
Mitochondria Stress Test
B
Wild-type
Bmpr1a-/-
Pyr 1 mM
OM 2.5 µM
FCCP 300 nM
R&A 6 µM
OCR (pmol O2/ min) per 100 000 cells
Time (minutes)
C
Wild-type
Bmpr1a-/-
OCR (pmol O2/ min) per 100 000 cells
Basal Respiration
ATP Production
Response to Pyruvate
Coupling Efficiency
Glycolysis Stress Test
D
Wild-type
Bmpr1a-/-
Glu 2.5 mM
Glu 10 mM
OM 2.5 µM
2-DG 50 mM
ECAR (mpH/min) per 100 000 cells
Time (minutes)
E
Wild-type
Bmpr1a-/-
ECAR (mpH/min) per 100 000 cells
Glycolytic Capacity
Glycolytic Reserve
Δψm
F
Separate culture
Co-culture
Wild-type
Bmpr1a-/-
Normalized To Mode
TMRM
Fold change (MFI vs control)
Separate
Co-culture
G
Separate culture
Co-culture
Wild-type
4n
Normalized To Mode
TMRM
Fold change (MFI vs control)
Separate
Co-culture
H
Hoechst
Bmpr1a-/- - GFP
Mitotracker Red
Merged
Δψm
Hoechst
Bmpr1a-/- - GFP
TOMM20
Merged
Mass
I
Wild-type
Bmpr1a-/-
15 KDa
TOMM20
50 KDa
α-tubulin
TOMM20 /α-tubulin
J
Wild-type
Bmpr1a-/-
37KDa
mt-CO1
150 KDa
Vinculin
mt-CO1 / vinculin
K
Normalized To Mode
TMRM
Wild-type
Bmpr1a-/-
Bmpr1a-/-; p53-/-
Fold change (MFI vs control)

Fig. 5

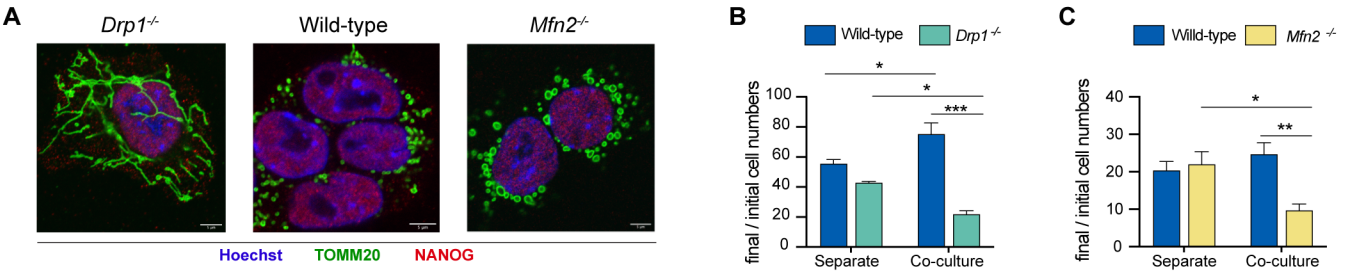
A
Drp1-/-
Wild-type
Mfn2-/-
Hoechst
TOMM20
NANOG
B
Wild-type
Drp1-/-
final / initial cell numbers
100
80
60
40
20
0
*
*
***
Separate
Co-culture
C
Willd-type
Mfn2 -/-
final / initial cell numbers
40
30
20
10
0
*
**
Separate
Co-culture

Fig. 6

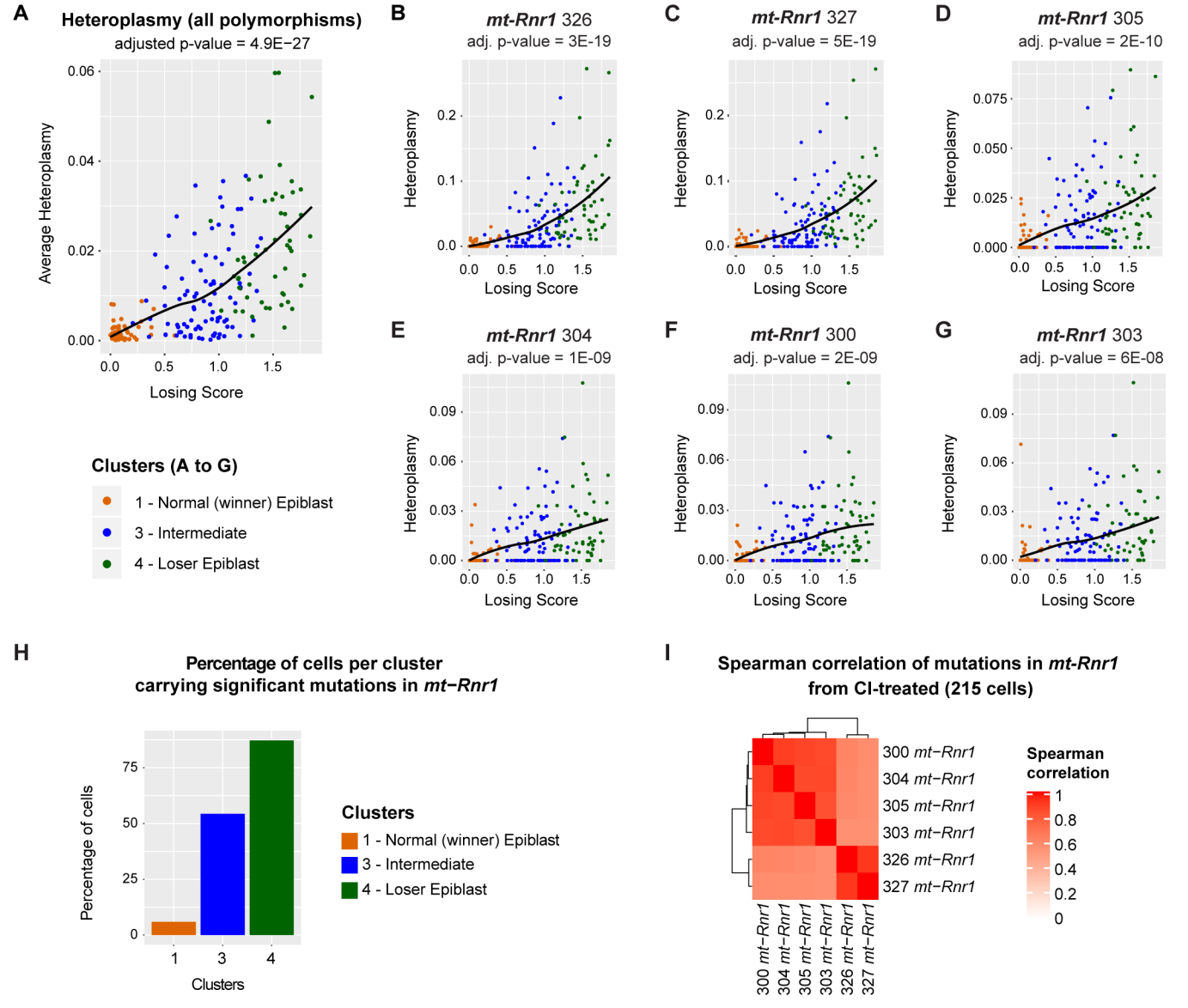
A
Heteroplasmy (all polymorphisms)
adjusted p-value = 4.9E−27
Average Heteroplasmy
Losing Score
B
mt-Rnr1 326
adj. p-value = 3E-19
C
mt-Rnr1 327
adj. p-value = 5E-19
D
mt-Rnr1 305
adj. p-value = 2E-10
E
mt-Rnr1 304
adj. p-value = 1E-09
F
mt-Rnr1 300
adj. p-value = 2E-09
G
mt-Rnr1 303
adj. p-value = 6E-08
Heteroplasmy
Losing Score
Clusters (A to G)
1 - Normal (winner) Epiblast
3 - Intermediate
4 - Loser Epiblast

H
Percentage of cells per cluster
carrying significant mutations in mt−Rnr1
Percentage of cells
Clusters
Clusters
1 - Normal (winner) Epiblast
3 - Intermediate
4 - Loser Epiblast
I
Spearman correlation of mutations in mt-Rnr1
from CI-treated (215 cells)
300 mt−Rnr1
304 mt−Rnr1
305 mt−Rnr1
303 mt−Rnr1
326 mt−Rnr1
327 mt−Rnr1
Spearman correlation

Fig. 7

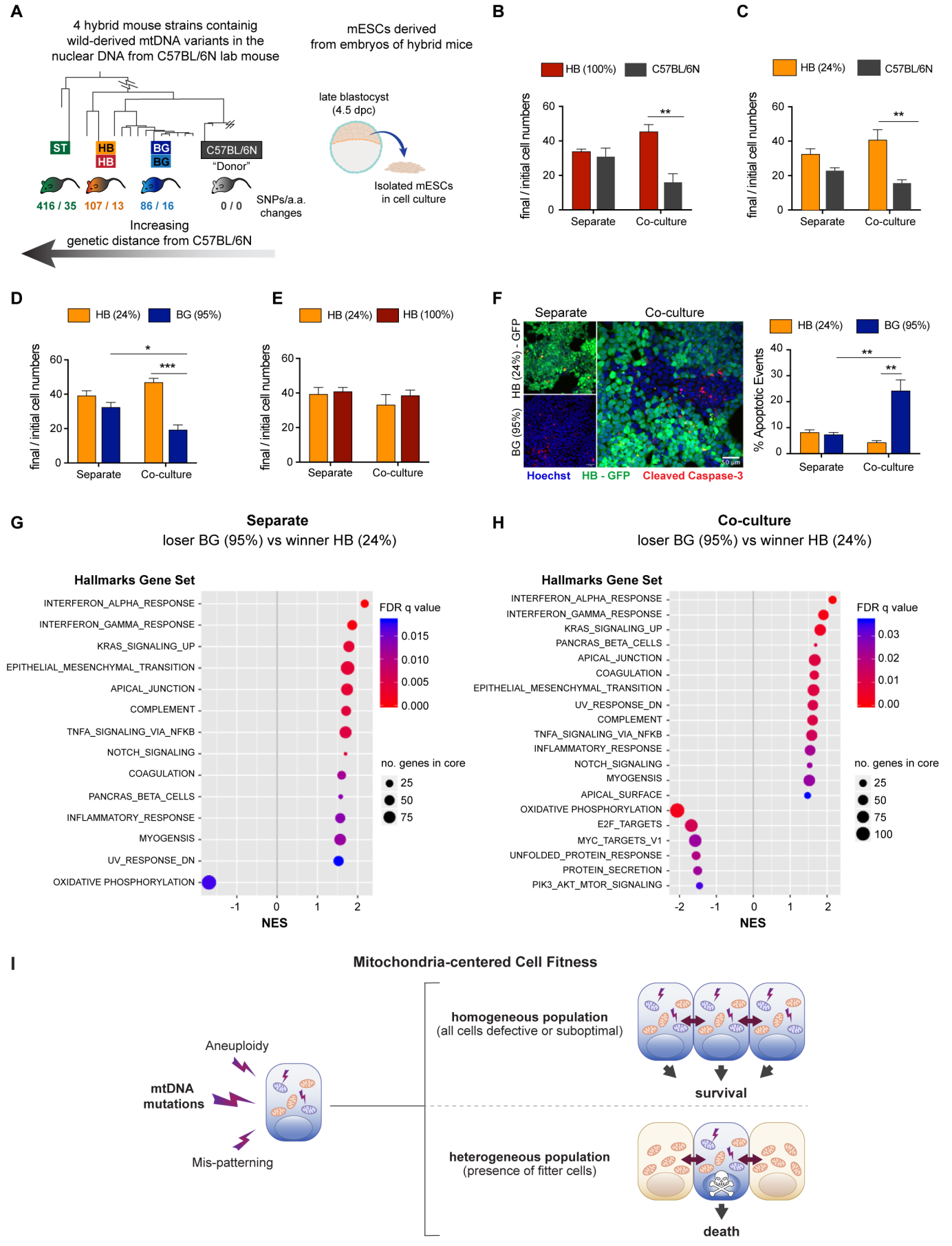
A
4 hybrid mouse strains containig wild-derived mtDNA variants in the nuclear DNA from C57BL/6N lab mouse
mESCs derived from embryos of hybrid mice
ST
HB HB
BG BG
C57BL/6N "Donor"
late blastocyst (4.5 dpc)
Isolated mESCs in cell culture
416 / 35
107 / 13
86 / 16
0 / 0
SNPs/a.a. changes
Increasing genetic distance from C57BL/6N
B
HB (100%)
C57BL/6N
final / initial cell numbers
Separate
Co-culture
C
HB (24%)
C57BL/6N
D
HB (24%)
BG (95%)
E
HB (24%)
HB (100%)
F
Separate
Co-culture
HB (24%) - GFP
BG (95%)
Hoechst
HB - GFP
Cleaved Caspase-3
% Apoptotic Events
G
Separate
loser BG (95%) vs winner HB (24%)
Hallmarks Gene Set
INTERFERON_ALPHA_RESPONSE
INTERFERON_GAMMA_RESPONSE
KRAS_SIGNALING_UP
EPITHELIAL_MESENCHYMAL_TRANSITION
APICAL_JUNCTION
COMPLEMENT
TNFA_SIGNALING_VIA_NFKB
NOTCH_SIGNALING
COAGULATION
PANCRAS_BETA_CELLS
INFLAMMATORY_RESPONSE
MYOGENSIS
UV_RESPONSE_DN
OXIDATIVE PHOSPHORYLATION
FDR q value
no. genes in core
NES
H
Co-culture
loser BG (95%) vs winner HB (24%)
Hallmarks Gene Set
INTERFERON_ALPHA_RESPONSE
INTERFERON_GAMMA_RESPONSE
KRAS_SIGNALING_UP
PANCRAS_BETA_CELLS
APICAL_JUNCTION
COAGULATION
EPITHELIAL_MESENCHYMAL_TRANSITION
UV_RESPONSE_DN
COMPLEMENT
TNFA_SIGNALING_VIA_NFKB
INFLAMMATORY_RESPONSE
NOTCH_SIGNALING
MYOGENSIS
APICAL_SURFACE
OXIDATIVE PHOSPHORYLATION
E2F_TARGETS
MYC_TARGETS_V1
UNFOLDED_PROTEIN_RESPONSE
PROTEIN_SECRETION
PIK3_AKT_MTOR_SIGNALING
FDR q value
no. genes in core
NES
I
Mitochondria-centered Cell Fitness
Aneuploidy
mtDNA mutations
Mis-patterning
homogeneous population
(all cells defective or suboptimal)
survival
heterogeneous population
(presence of fitter cells)
death

Fig. S1

A

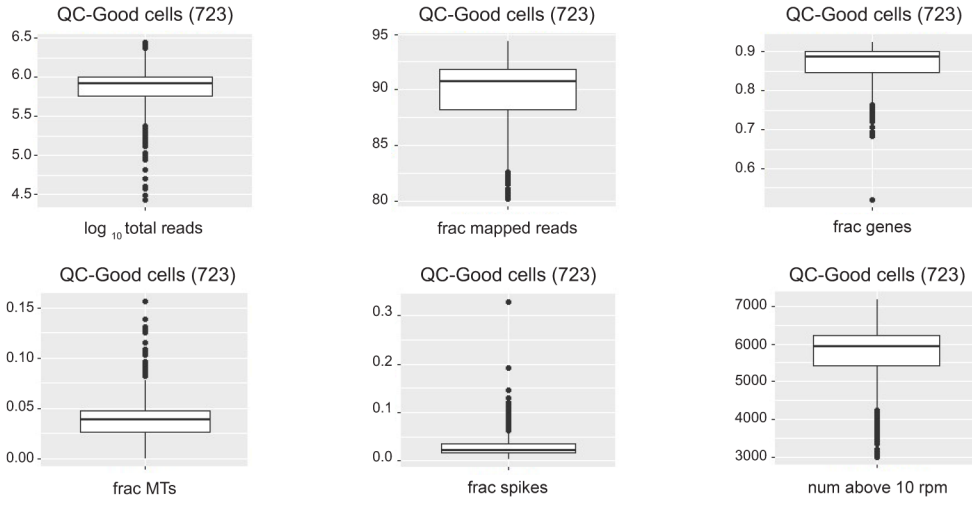

B

Condition\Batch	1	2	3	4	5
CI-treated	136	105	86	16	24
DMSO	132	110	78	15	21

C

Cluster/Batch	1	2	3	4	5
1	147	81	57	7	15
2	45	65	44	7	10
3	46	34	35	13	6
4	23	18	21	2	7
5	7	17	7	2	7

D

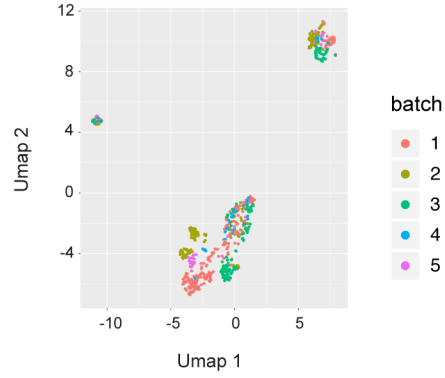

Fig. S2

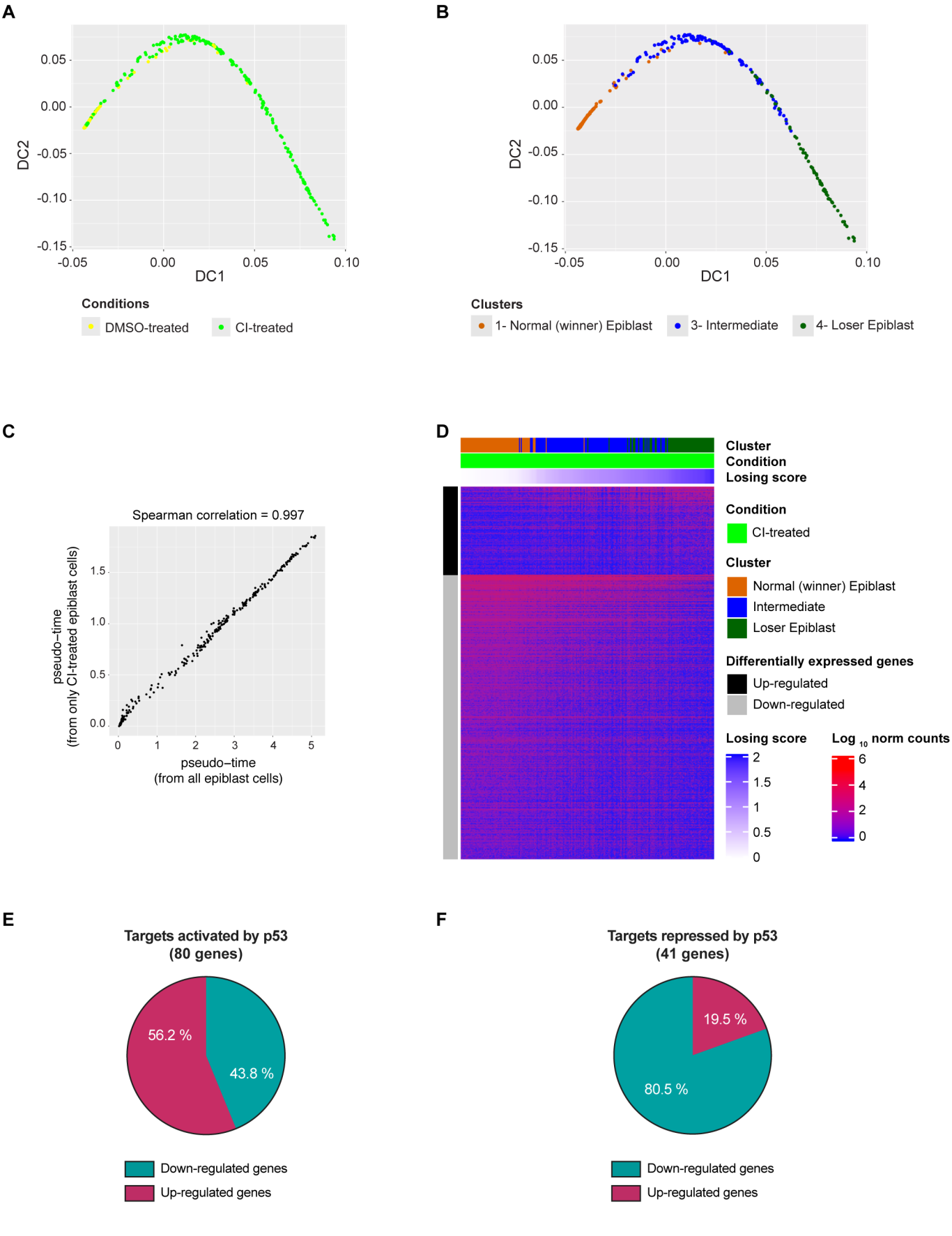
A
0.05
0.00
-0.05
-0.10
-0.15
DC2
-0.05
0.00
0.05
0.10
DC1
Conditions
DMSO-treated
CI-treated
B
0.05
0.00
-0.05
-0.10
-0.15
DC2
-0.05
0.00
0.05
0.10
DC1
Clusters
1- Normal (winner) Epiblast
3- Intermediate
4- Loser Epiblast
C
Spearman correlation = 0.997
pseudo−time
(from only CI-treated epiblast cells)
1.5
1.0
0.5
0.0
0
1
2
3
4
5
pseudo−time
(from all epiblast cells)
D
Cluster
Condition
Losing score
Condition
CI-treated
Cluster
Normal (winner) Epiblast
Intermediate
Loser Epiblast
Differentially expressed genes
Up-regulated
Down-regulated
Losing score
2
1.5
1
0.5
0
Log 10 norm counts
6
4
2
0
E
Targets activated by p53
(80 genes)
56.2 %
43.8 %
Down-regulated genes
Up-regulated genes
F
Targets repressed by p53
(41 genes)
19.5 %
80.5 %
Down-regulated genes
Up-regulated genes

Fig. S3

A

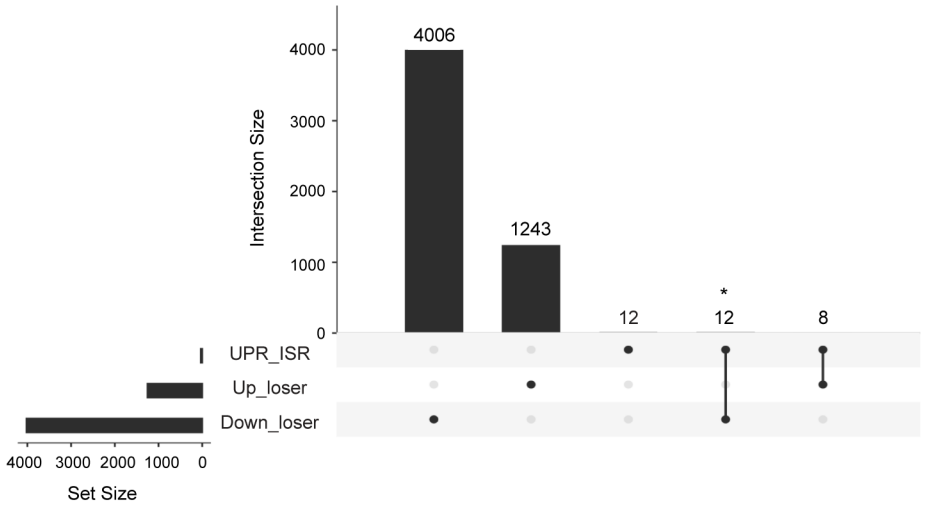

B

Gene	FDR	Rank
Ddit3	4.63E-39	2
Atf3	6.08E-27	22
Atf4	2.14E-23	31
Foxo3	2.69E-22	37
Ppp1r15a	8.33E-18	68
Eif2ak3	7.17E-13	150
Nfe2l2	1.55E-10	207
Gdf15	5.53E-08	333

C

Gene	FDR	Rank
Mthfd1l	2.54E-35	147
Hspe1	8.71E-34	164
Cat	2.44E-30	219
Hspd1	6.93E-13	1262
Sod2	1.25E-10	1551
Hsph1	4.48E-10	1655
Lonp1	1.08E-06	2348
Eif2a	1.49E-06	2382
Mthfd2	1.31E-05	2693
Hspa4	2.84E-05	2790
Cth	2.53E-03	3677
Nrf1	2.86E-03	3698

D

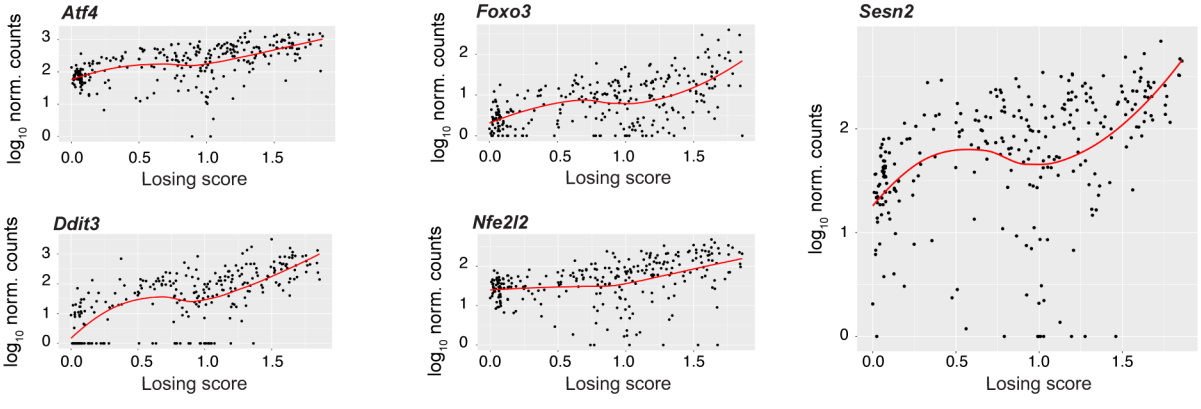

E

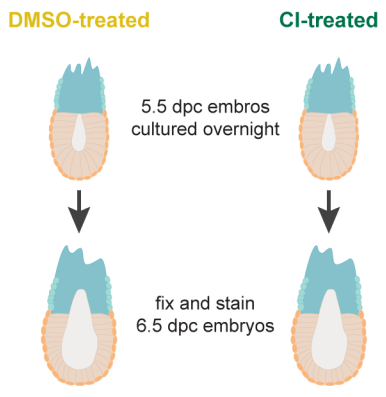

F

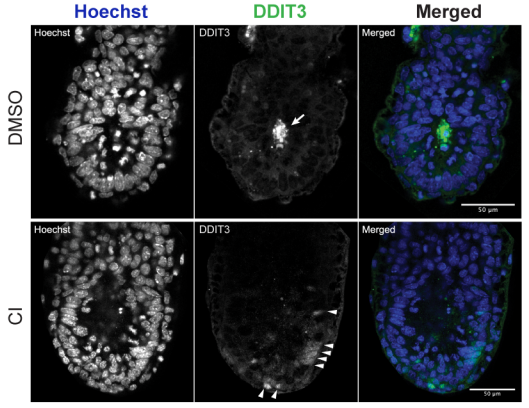

G

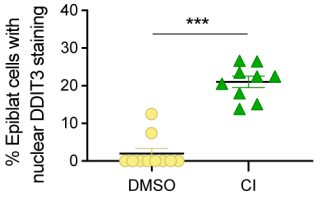

Fig. S4

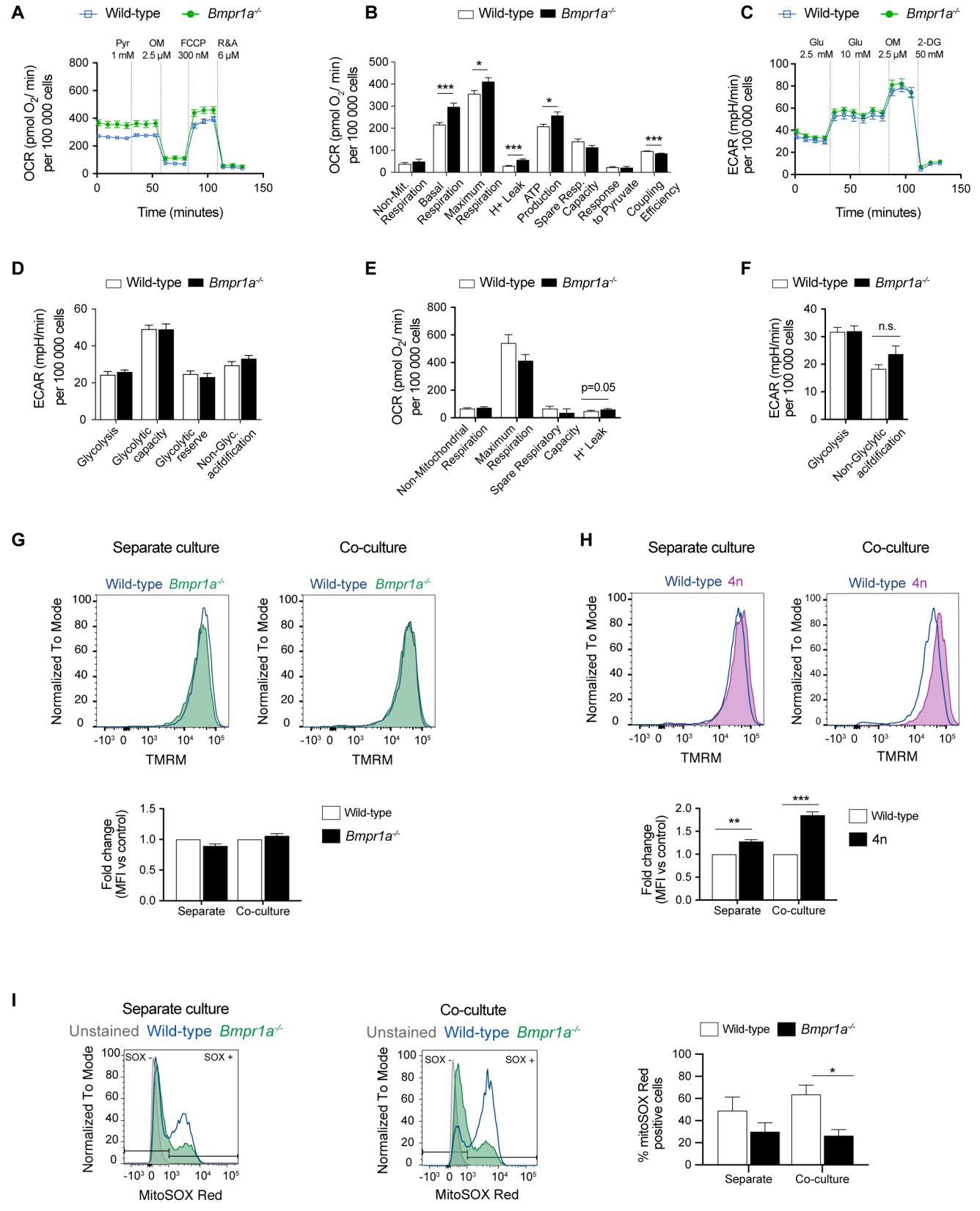
A
Wild-type
Bmpr1a-/-
Pyr 1 mM
OM 2.5 µM
FCCP 300 nM
R&A 6 µM
OCR (pmol O2/ min) per 100 000 cells
Time (minutes)
B
Wild-type
Bmpr1a-/-
OCR (pmol O2/ min) per 100 000 cells
Non-Mit. Respiration
Basal Respiration
Maximum Respiration
H+ Leak
ATP Production
Spare Resp. Capacity
Response to Pyruvate
Coupling Efficiency
C
Wild-type
Bmpr1a-/-
Glu 2.5 mM
Glu 10 mM
OM 2.5 µM
2-DG 50 mM
ECAR (mpH/min) per 100 000 cells
Time (minutes)
D
Wild-type
Bmpr1a-/-
ECAR (mpH/min) per 100 000 cells
Glycolysis
Glycolytic capacity
Glycolytic reserve
Non-Glyc. acidification
E
Wild-type
Bmpr1a-/-
OCR (pmol O2/ min) per 100 000 cells
p=0.05
Non-Mitochondrial Respiration
Maximum Respiration
Spare Respiratory Capacity
H+ Leak
F
Wild-type
Bmpr1a-/-
n.s.
ECAR (mpH/min) per 100 000 cells
Glycolysis
Non-Glycolytic acidification
G
Separate culture
Co-culture
Wild-type
Bmpr1a-/-
Normalized To Mode
TMRM
Fold change (MFI vs control)
Separate
Co-culture
H
Separate culture
Co-culture
Wild-type
4n
Normalized To Mode
TMRM
Fold change (MFI vs control)
Separate
Co-culture
I
Separate culture
Co-cultute
Unstained
Wild-type
Bmpr1a-/-
SOX -
SOX +
Normalized To Mode
MitoSOX Red
% mitoSOX Red positive cells
Separate
Co-culture

Fig. S5

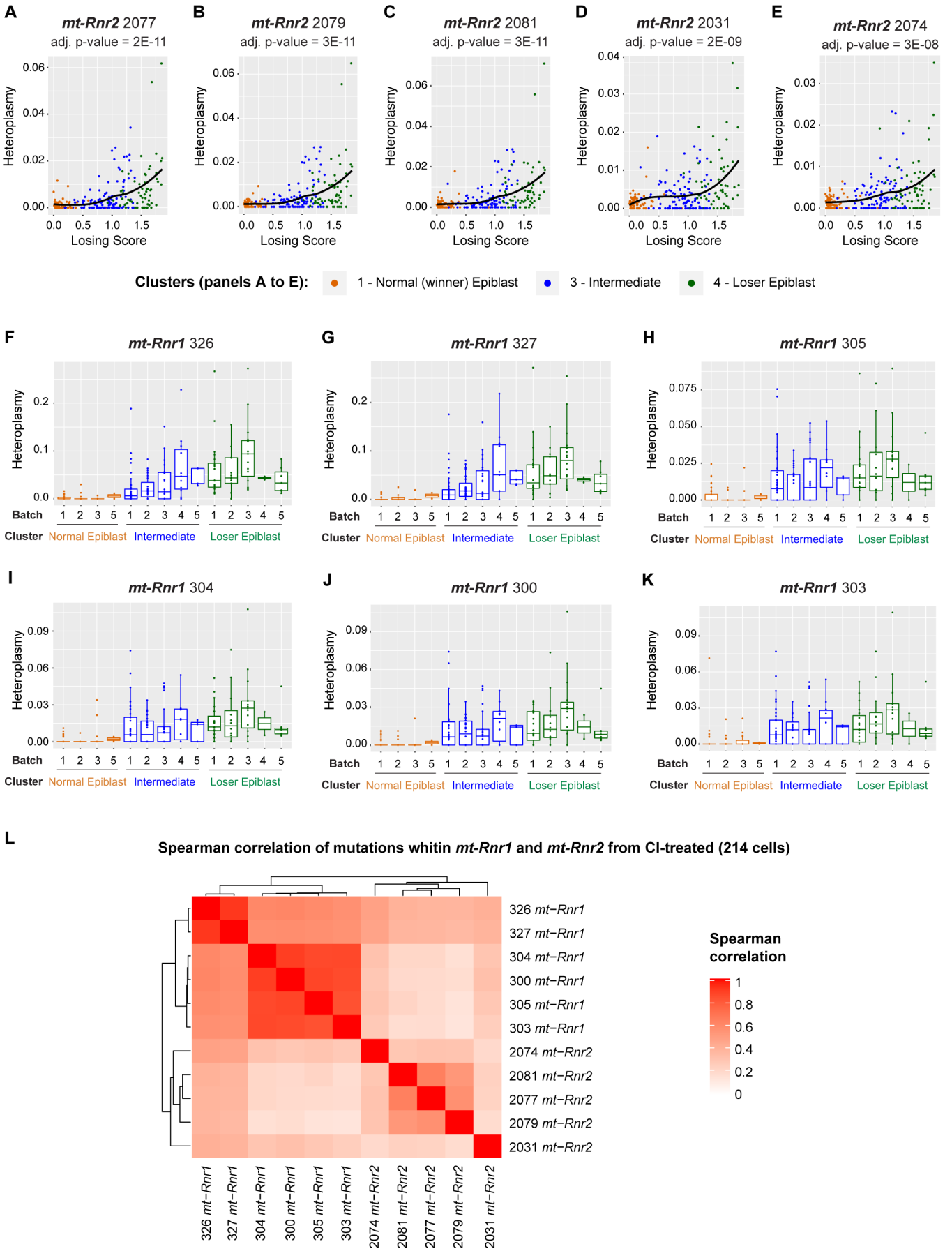
A
mt-Rnr2 2077
adj. p-value = 2E-11
B
mt-Rnr2 2079
adj. p-value = 3E-11
C
mt-Rnr2 2081
adj. p-value = 3E-11
D
mt-Rnr2 2031
adj. p-value = 2E-09
E
mt-Rnr2 2074
adj. p-value = 3E-08
Heteroplasmy
Losing Score
Clusters (panels A to E):
1 - Normal (winner) Epiblast
3 - Intermediate
4 - Loser Epiblast
F
mt-Rnr1 326
G
mt-Rnr1 327
H
mt-Rnr1 305
I
mt-Rnr1 304
J
mt-Rnr1 300
K
mt-Rnr1 303
Batch
Cluster
Normal Epiblast
Intermediate
Loser Epiblast
L
Spearman correlation of mutations whitin mt-Rnr1 and mt-Rnr2 from CI-treated (214 cells)
326 mt−Rnr1
327 mt−Rnr1
304 mt−Rnr1
300 mt−Rnr1
305 mt−Rnr1
303 mt−Rnr1
2074 mt−Rnr2
2081 mt−Rnr2
2077 mt−Rnr2
2079 mt−Rnr2
2031 mt−Rnr2
Spearman correlation

Fig. S6

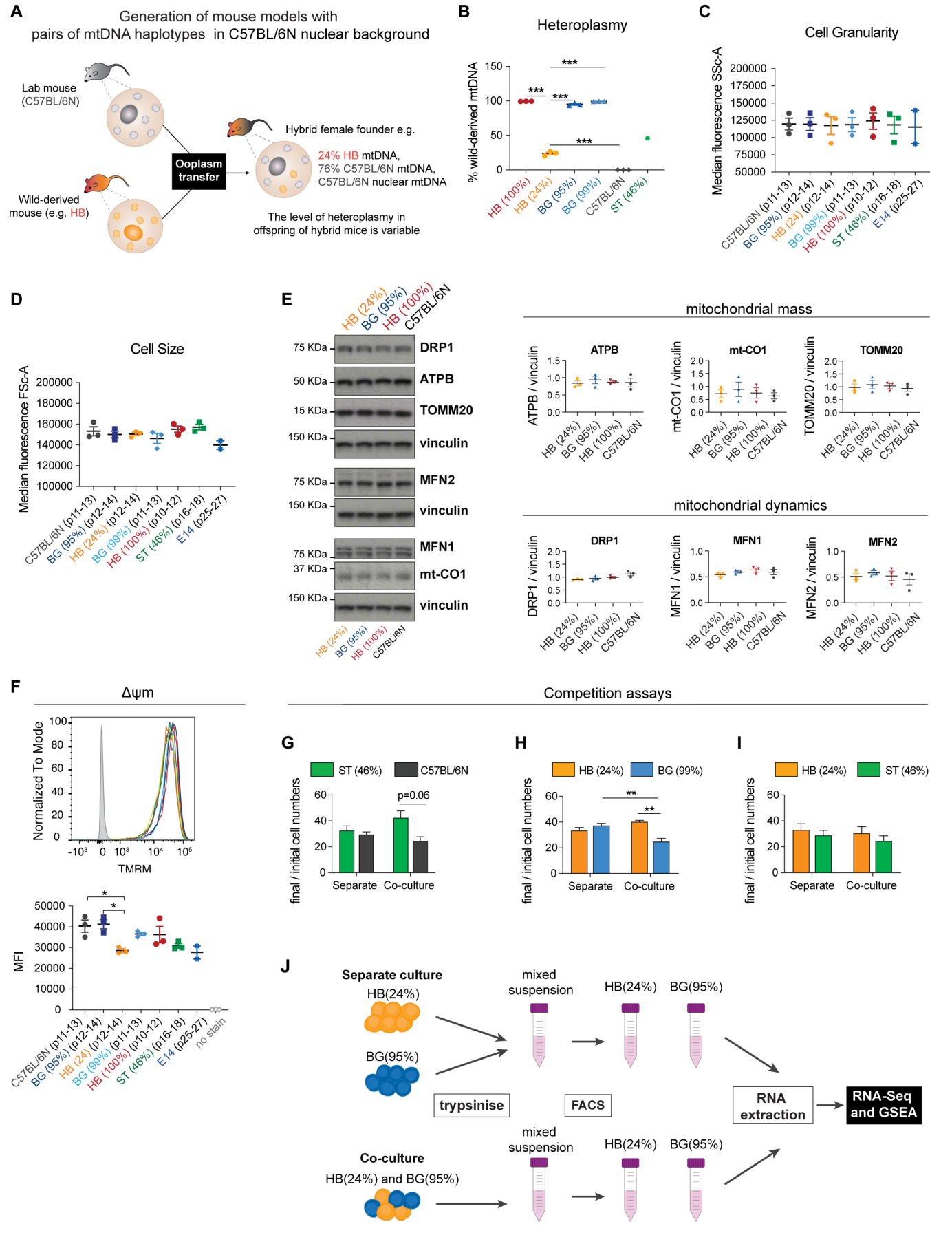
A
Generation of mouse models with
pairs of mtDNA haplotypes in C57BL/6N nuclear background
Lab mouse
(C57BL/6N)
Wild-derived
mouse (e.g. HB)
Ooplasm
transfer
Hybrid female founder e.g.
24% HB mtDNA,
76% C57BL/6N mtDNA,
C57BL/6N nuclear mtDNA
The level of heteroplasmy in
offspring of hybrid mice is variable
B
Heteroplasmy
% wild-derived mtDNA
HB (100%)
HB (24%)
BG (95%)
BG (99%)
C57BL/6N
ST (46%)
C
Cell Granularity
Median fluorescence SSc-A
D
Cell Size
Median fluorescence FSc-A
E
HB (24%)
BG (95%)
HB (100%)
C57BL/6N
75 KDa
DRP1
50 KDa
ATPB
15 KDa
TOMM20
150 KDa
vinculin
75 KDa
MFN2
150 KDa
vinculin
75 KDa
MFN1
37 KDa
mt-CO1
150 KDa
vinculin
mitochondrial mass
ATPB
ATPB / vinculin
mt-CO1
mt-CO1 / vinculin
TOMM20
TOMM20 / vinculin
mitochondrial dynamics
DRP1
DRP1 / vinculin
MFN1
MFN1 / vinculin
MFN2
MFN2 / vinculin
F
Δψm
Normalized To Mode
TMRM
MFI
no stain
Competition assays
G
ST (46%)
C57BL/6N
p=0.06
final / initial cell numbers
Separate
Co-culture
H
HB (24%)
BG (99%)
I
HB (24%)
ST (46%)
J
Separate culture
HB(24%)
BG(95%)
mixed
suspension
trypsinise
FACS
RNA
extraction
RNA-Seq
and GSEA
Co-culture
HB(24%) and BG(95%)

Fig. S7

A

Source	Term	Adjusted p-value
GO:CC	mitochondrial protein complex	5.91E-05
GO:CC	inner mitochondrial membrane protein complex	8.84E-04
GO:CC	mitochondrial inner membrane	8.93E-04
GO:CC	mitochondrial respirasome	2.44E-03
GO:CC	respiratory chain complex	3.89E-03
GO:CC	respirasome	6.50E-03
GO:CC	mitochondrial part	1.06E-02
GO:CC	organelle inner membrane	4.65E-02
KEGG	oxidative phosphorylation	7.71E-04
KEGG	Huntington disease	2.35E-03
WP	electron transport chain	1.26E-03

B

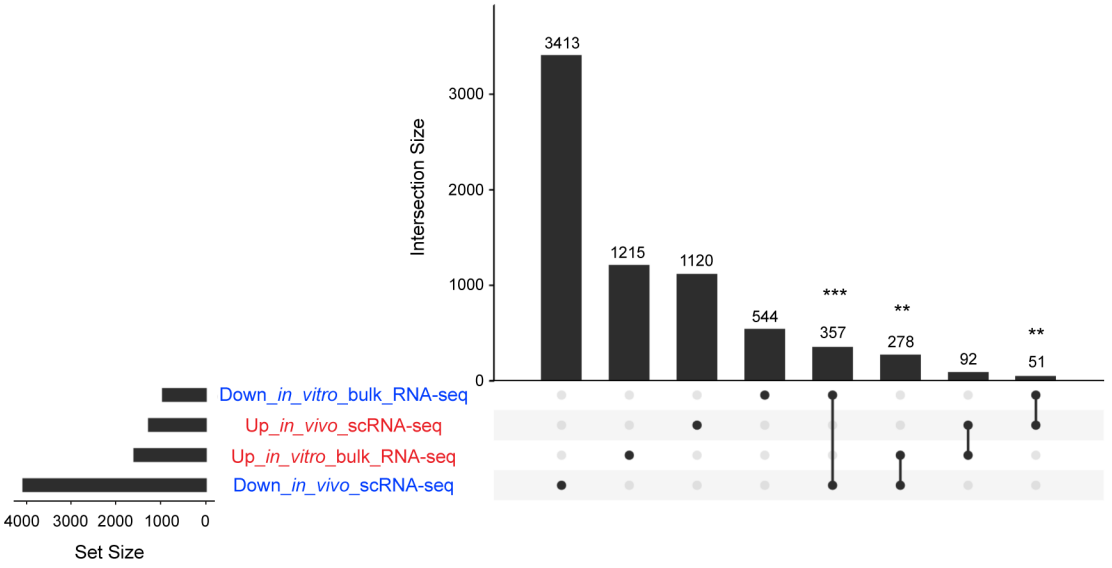

C